İSTANBUL TECHNICAL UNIVERSITY ★ INSTITUTE OF SCIENCE AND TECHNOLOGY

TITANIUM MICROMACHINING BY FEMTOSECOND LASER

M.Sc. Thesis by
Vural KARA

Department : Advanced Technologies

Programme : Material Science and Engineering

JUNE 2011

İSTANBUL TECHNICAL UNIVERSITY ★ INSTITUTE OF SCIENCE AND TECHNOLOGY

TITANIUM MICROMACHINING BY FEMTOSECOND LASER

M.Sc. Thesis by
Vural KARA
(521091033)

Date of submission : 06 May 2011
Date of defence examination: 07 June 2011

Supervisor (Chairman) : Assist.Prof. Dr. Hüseyin KIZIL (ITU)
Members of the Examining Committee : Assoc.Prof. Dr. Levent TRABZON(ITU)
Prof. Dr. Eyüp Sabri KAYALI (ITU)

JUNE 2011

İSTANBUL TEKNİK ÜNİVERSİTESİ ★ FEN BİLİMLERİ ENSTİTÜSÜ

FEMTOSANİYE LAZER İLE TİTANYUM MİKROİŞLEME

YÜKSEK LİSANS TEZİ
Vural KARA
(521091033)

Tezin Enstitüye Verildiği Tarih : 06 Mayıs 2011
Tezin Savunulduğu Tarih : 07 Haziran 2011

Tez Danışmanı : Yrd. Doç. Dr. Hüseyin KIZIL(İTÜ)
Diğer Jüri Üyeleri : Doç. Dr. Levent TRABZON (İTÜ)
Prof. Dr. Eyüp Sabri KAYALI (İTÜ)

HAZİRAN 2011

FOREWORD

I would like to express my deep appreciation and thanks for my advisor Assist. Prof. Dr. Hüseyin KIZIL. With this thesis, I meet a new research area and conducted an experimental study in diverse laboratories. These opportunities provided me to gain different experiences. He always supported me to pursue an interdisciplinary study. Also, I would like to thank Assoc. Prof. Dr. Levent TRABZON, who was always with me with his kind suggestions and support.

During my thesis, my friend Electronic Engineer Omid Tayefeh GHALEHBEYGI helped me in my experiments. He stayed with me in laboratory with his willing, even at nights and at weekends. I would like to express my thanks to him for all his help and support. Also I want to thank, Electronic Engineer Berat DOGAN for taking photos by Scanning Electron Microscope.

Lasers and their material interaction principles are somewhat difficult for a mechanical engineer since their fundamentals are mostly based on modern physics and modern optics. Therefore, from the commencing of this thesis, Assoc. Prof. Dr. Selçuk AKTÜRK has supported and guided me patiently. I would like to express my deep appreciation and thanks for him for all his help.

June 2011

Vural Kara

Mechanical Engineer

TABLE OF CONTENTS

Page

ABBREVIATIONS

CCD	**:** Charge Coupled Device
fs	**:** Femtosecond
FWHM	**:** Full With at Half Maximum
HAZ	**:** Heat Affected Zone
ns	**:** Nanosecond
SEM	**:** Scanning Electron Microscope
YAG	**:** Yttrium Aluminium Garnet

LIST OF TABLES

Page

LIST OF FIGURES

Page

TITANIUM MICROMACHINING BY FEMTOSECOND LASER

SUMMARY

In the last two decades, there is a rapid increase in the femtosecond laser applications. Since this type of lasers produce ultrashort pulse durations, which means high peak powers can be obtained, they provide unique advantages. Also, nanoscale science requires structures, which are not possible to fabricate by conventional technologies. Recently, femtosecond lasers are getting a good attention by many researchers in diverse applications such as precise hole drilling, microchannel cutting, micro/nanostructuring, and biomedical devices using metals, semiconductors, composites and transparent materials.

In this thesis, a femtosecond laser is used in order to micromachine titanium, which is a widely used material in industrial and biomedical applications due to its exceptional properties. Several experiments performed systematically in order to characterize the ablation depth with pulse energy, translation speed, and the consecutive passes over the channels. The main purpose of this study is to obtain the optimum parameters to cut, smooth microscale channels without accumulated debris. During the study, formations of microcolumns, called spikes, are also observed on titanium surface which can enhance biomedical implants' performance in human body, and these could be used as traps so as to capture specific cells in the microchannels for various biological studies.

The characteristics of the ablation depth as a function of cut parameters are investigated and channels having smooth surfaces are obtained. Moreover, the reason behind the formations of microcolumns is discussed.

FEMTOSANİYE LAZER İLE TİTANYUM MİKROİŞLEME

ÖZET

Geçtiğimiz son 20 yıl içerisinde femtosaniye lazerlerin uygulama alanlarında hızlı bir artış gözlemlenmektedir. Bu tip lazerler çok kısa süreli darbeler ürettikleri için çok yüksek güç değerlerine ulaşabilmekte ve bu da eşsiz avantajlar sağlamaktadır. Ayrıca nanobilim çok küçük ölçekli yapıların, partiküllerin üretilmesini gerektirmektedir ki bu da geleneksel teknolojilerle pratik olmamaktadır. Bu nedenle, femtosaniye lazerler geleneksel mikroişleme yöntemlerine iyi bir rakip olmaktadır.

Femtosaniye lazer ile mikroişlemenin çok hızlı genişleyen uygulama alanları bulunmaktadır. Çeşitli malzemeler, örneğin metaller, yarıiletkenler, transparant malzemeler, kompozitler femtosaniye lazerlerle işlenebilmektedir. Çok kısa süreli darbeler üretmesinden dolayı, lazer hüzmesi ile malzemenin etkileştiği bölgenin etrafına zarar verilmemektedir. Bu açıdan femtosaniye lazerlerin, hassas delik delme, kesme, mikro/nano yapılandırma ve biyomedikal cihazların üretimi gibi önemli uygulama alanları bulunmaktadır.

Bu tez çalışmasında, sanayide ve biyomedikal uygulamalarda çok iyi özelliklerinden dolayı sıkça kullanılan, titanyum malzemesi femtosaniye lazer ile mikroişlenmiştir. Sistematik bir şekilde deneyler yapılmış ve ablasyon derinliği, darbe enerjisi, tarama hızı ve tekrarlı taramalar ile karakterize edilmiştir. Dolayısıyla, tezin amacı, ablasyon derinliğinin, değişen parametreler ile karakteristiğini ortaya koymak ve pürüzsüz kanalların açılması için gerekli olan optimum parametreleri elde edebilmektir. Ayrıca, titanyum yüzeyinde ve kanalların içerisinde mikroyapıların oluşumu gözlemlenmiştir. Bu yapılar biyomedikal implantların vücut içerisindeki dayanımını ve performansını arttırmakta, ayrıca mikro kanallar içerisinde hücre ayrıştırması için tuzak olarak kullanılabilmektedir.

Sonuç olarak bu tez çalışması kapsamında ablasyon derinliğinin, değişen parametrelerle olan karakteristiği ortaya konulmuş ve pürüzsüz kanallar açılmıştır. Ayrıca, mikro yapıların oluşum sebepleri irdelenmiştir.

1. INTRODUCTION

Femtosecond lasers produce pulses in femtosecond range (10^{-15} s) which can ablate a material without causing any damage on the laser material interaction surroundings. Femtosecond laser micromachining applications increase rapidly due to its unique advantages over conventional fabrication techniques. The basic features of the femtosecond pulses are summarized by *Nolte et.al.* [1]:

- Rapid energy deposition and creation of vapour and plasma phases
- Absence of the molten material
- Negligible heat-affected zones (HAZ).

There are many studies about the physical mechanism of the interaction of laser pulses with absorptive [2-4] and transparent materials [4-6]. The ablation process takes place in both of these materials and has potential applications in industry and in research groups.

In literature, femtosecond laser micromachining for hole drilling and cutting of, semiconductors [7-12], metals [1,13-17], and transparent materials [5,6,18-24], can be found. Moreover, morphological changes of absorptive [25-28] and transparent [29-34] materials by femtosecond lasers are studied.

Titanium is a widely used material in industrial and biomedical applications due to its high durability, high strength, light weight, biocompatibility, and good mechanical performance in human body [35-37]. Several experiments performed on titanium surface to fabricate textures at microscale by femtosecond laser pulses. The purpose of this application is to enhance titanium implants stability and the strength of the bone/implant interface [35-41]. However the mechanisms behind the formation of these micro columns, which are generally called as “spikes” [48,49,52], are not fully understood.

In this thesis, the optimum laser parameters are investigated for micromachining of titanium to obtain smooth micro channels. A systematic series of experiments are performed in order to characterize the ablation depth with pulse energy, translation speed and consecutive number of pulses. In addition, the formations of the microcolumns are observed and some experiments are performed in order to discover their reproducibility.

2. FEMTOSECOND LASER MICROMACHINING

2.1 Femtosecond Laser-Material Interaction

Laser micromachining results in material removal. This happens through the ablation process where the test specimen under laser irradiation absorbs laser energy and converts it to the liquid or vapour. The laser ablation takes place either linear absorption or nonlinear absorption [4,42-44].

2.1.1 Absorption and ionization

2.1.1.1 Linear absorption

The absorption process in materials take place with the aid of free and valance electrons, if the materials' bandgap is smaller than laser photon energy [45]. In non-metallic materials the highest level of the valance band is occupied by an electron. If the photon energy exceeds the bandgap energy, light can be absorbed by the material, and electrons are promoted to the conduction band [43].

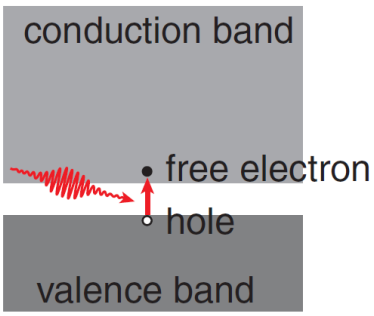

Figure 2.1 : Photon is absorbed by electron and promoting itself to the conduction band [43].

In metals, in contrast, the conduction band is partially occupied. Free electrons can absorb photons and they gain momentum through an interaction with a phonon (a lattice vibration) to promote to a higher-lying level in the conduction band [43]. As a result, the material ablation can take place if the sufficient energy is deposited on the material surface.

2.1.1.2 Nonlinear absorption

In transparent materials, a single photon has not enough energy to excite an electron from valance band to conduction band. Therefore, absorption of laser energy can take place with nonlinear absorption. There are two excitation mechanisms in nonlinear absorption, photoionization and avalanche ionization [5,42,43]. In Photoionization electrons are directly excited by the laser field. There are two different regimes of photoionization, the multiphoton ionization and tunnelling ionization which both are related with laser frequency and intensity [42,43].

In tunnelling ionization, the laser electric field provides the electron to tunnel out from its potential to become free electron. This ionization is possible in strong laser fields and low laser frequency. At higher laser frequencies nonlinear photoionization take place by simultaneous absorption of multiple photons by an electron. The sum of the energy of all the photons absorbed must exceed the bandgap energy in order to achieve multiphoton ionization [42,43].

Avalanche ionization take place with the aid of "seed" electrons, which are always present in materials as free or conduction electrons. These seed electrons are result of metallic impurities, thermal or linear optical ionization of shallow energy levels of inclusions [4]. An electron in the conduction band absorbs several laser photons and when its energy exceeds the conduction band minimum by more than the bandgap energy, and then collisionally ionizes another electron, leaving two electrons at the conduction band minimum. As long as the laser field is present this process repeats, and the electron density in the conduction band grows exponentially [4,42,43].

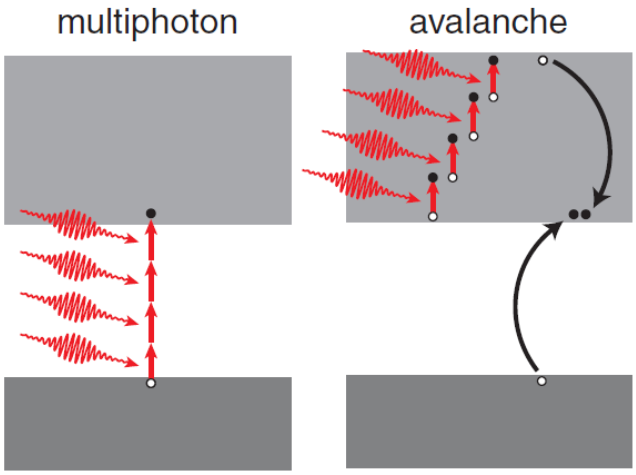

Figure 2.2 : Schematic diagram of multiphoton and avalanche ionization [43]

2.1.2 Pulse duration effect

The absorption of the laser beam can be expressed by two characteristic lengths. One is the optical penetration depth, which is the distance within which the photon energy is absorbed and can be written as [45]

$$\delta = \frac{1}{\alpha} \tag{2.1}$$

where α is the optical parameters of materials. The second length is the heat diffusion length, which is the distance of the thermal energy, which is conducted during the pulse, and can be written as [45]

$$l_{th} = \sqrt{\kappa \tau_p} \tag{2.2}$$

where τ_p is the pulse duration κ is the thermal diffusivity.

2.1.2.1 Long pulse interaction

For long pulses, since the fluence threshold varies as the square root of the pulse duration, the material heated by the beam pulse depends on the heat diffusion length. When the material and long pulse interacts, significant amount of material is melted, and ablation process take place with the liquid and vapor phase of the material. The non-ablated material resolidifies around the ablated region and prevents precise machining [45]. Most of the materials thermal diffusivity fluctuates between 0.1-1 cm^2/s [46].This indicates that for 10 ns pulse duration, heat wave will travel about 0.1-1 μm. This is longer than the optical penetration depth, which is approximately 10 nm for metals [43].

2.1.2.2 Short pulse interaction

For short pulses in the range of picosecond or femtosecond, the heat diffusion length will be equal or be much smaller than the optical penetration depth. Since the deposited energy is localized, the material in this region is quickly reaches the vaporization temperature. Thus, this provides more precise and cleaner cuts [45].

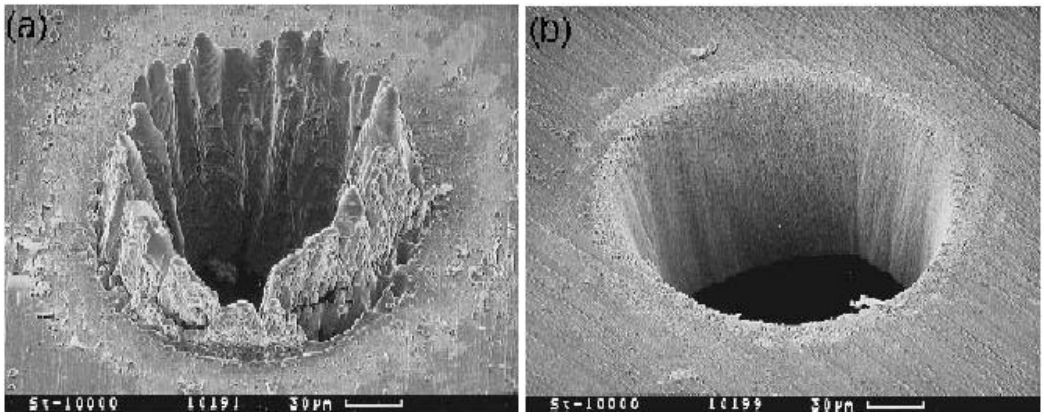

Figure 2.3 : Holes drilled on steel (a) pulse duration is 3.3 *ns* and fluence is 4.2 J/cm^2 (b) pulse duration is 200 *fs* and fluence is 0.5 J/cm^2 [28].

Figure 2.3 illustrates the pulse duration effect on the material processing. In Figure 2.3a the hole is drilled by 4.2 J/cm^2 , with 3.3 *ns* pulse duration, whereas in Figure 2.3b the material is drilled by 0.5 J/cm^2 with 200 *fs* pulse duration [28]. It is obvious that the pulse duration in femtosecond region has a significant effect on the material processing that there is no trace of the solidified material around the hole. Also as compared to nanosecond pulse regime, the heat-affected zone is not created and the quality of the holes inside is incomparable.

2.2 Applications of Femtosecond Laser Micromachining

2.2.1 Industrial applications

2.2.1.1 Femtosecond laser drilling and cutting

It is difficult to create small holes with diameters less than 100 μm by conventional micromachining techniques. It is therefore femtosecond lasers are a good solution for these applications such as fuel injection nozzles in automotive industry, hydraulic and pneumatic components. There is an example of injection nozzle which is drilled by femtosecond laser in Figure 2.4 [47]. As seen from the figure that the hole has a smooth surface without accumulated debris. Although laser drilling is performed in high fluences, high quality processing achieved.

The reason behind this can be divided in two steps. In the first step, high intensities are used rapidly drill a deep hole. Due to the characteristic of Gaussian laser beam, high intensity part of the laser pulse do not interact with the walls and propagates through the hole. On the other hand, the other parts of the laser pulse, which exhibit much low fluence as a result of Gaussian beam characteristic, interact with the walls. As a consequence, this low-fluence, interacts with walls, can be considered as "integrated" post-processing step, which provides high quality holes [13].

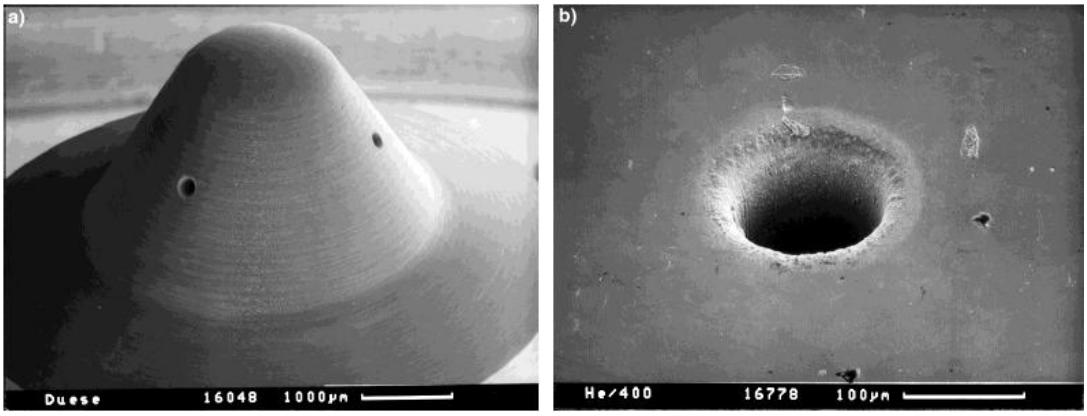

Figure 2.4 : (a) Cap of a injection nozzle (b) Magnified view of hole [47].

Femtosecond laser cutting provides unique applications such as microchannels in diverse materials such as glass[21,22], semiconductors [8-10] with small sizes. There are systematic studies performed in silicon [9] and in InP [10] and in both studies high quality channels are cut by femtosecond laser and some of the channels are indicated in Figure 2.5 and Figure 2.6.

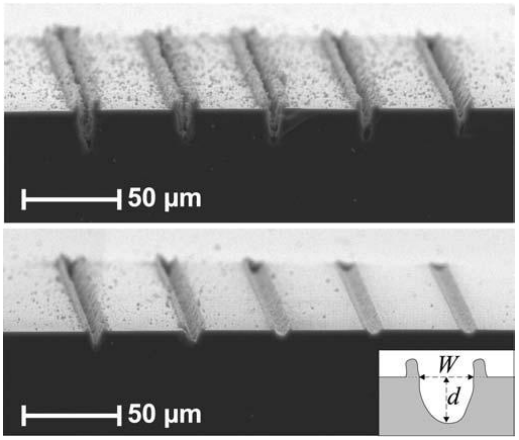

Figure 2.5 : Microchannels on silicon surface which are cut by fs laser [9].

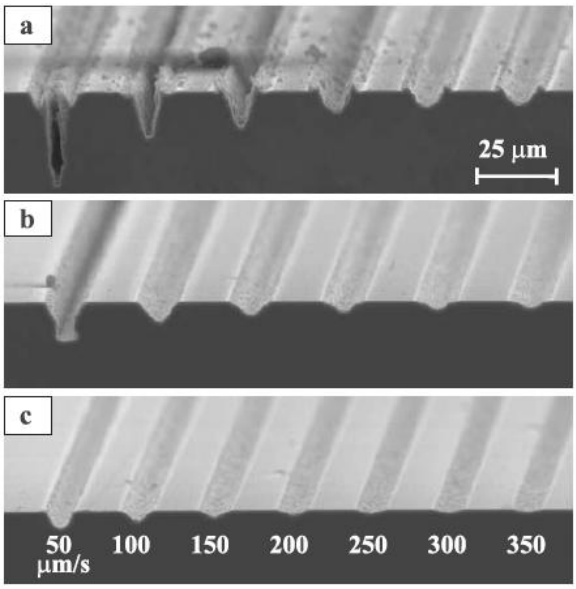

Figure 2.6 : Microchannels on InP surface which are cut fs laser [10].

Both these experiments illustrated in Figure 2.5 and Figure 2.6 are performed in same university by different group members. They pursue a systematic study and characterize the ablation depth with pulse energy, translation speed and consecutive passes. There are some accumulated pulses in silicon, whereas the InP channels do not include debris around and inside the channels. It is obvious from figures that smooth channels can be cut by femtosecond lasers.

2.2.1.2 Femtosecond laser micro/nanostructuring

Structuring of materials surfaces provides technological importance since they can be used for fluid sterilization, cell encapsulation, drug delivery etc. In this technique the laser pulses are directly send to the materials surfaces which create micro/nano structures. Thus it has some advantages since laser processing provides reproducibility and less contamination due to its non-contact process. The morphology of these structures depends on the laser processing parameters; number of incident laser pulses, fluence, wavelength, pulse duration, and the ambient atmosphere and pressure [37,41].

For the last two decade, the most studies in this area is performed in silicon [48-52], since it is a widely used material in microelectronics industry. Figure 2.6 illustrates a study performed by *Her et.al.* [52] shows the micro columns, which are called spikes, on silicon surface. *Sarnet et.al.* stated that these micro columns in silicon improve the solar cell efficiency since they reduce the incident solar light reflection and a microstructured silicon part is shown in Figure 2.7 [53].

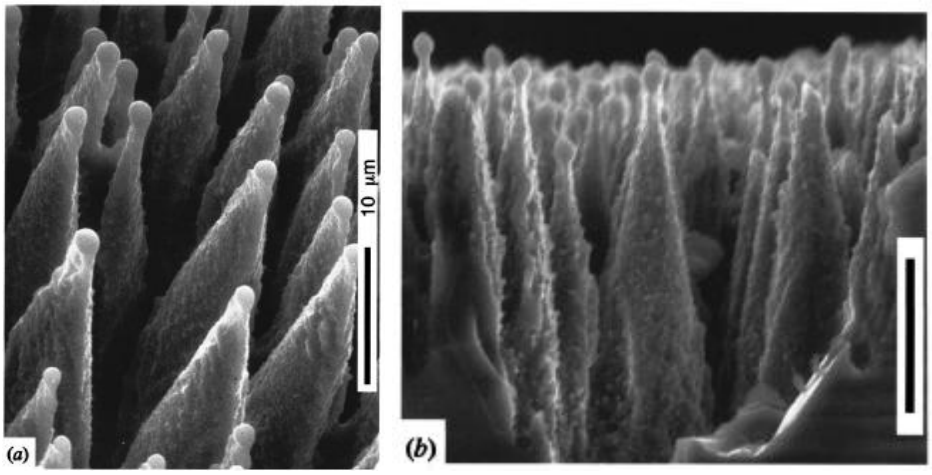

Figure 2.7 : Spikes on silicon surface [52].

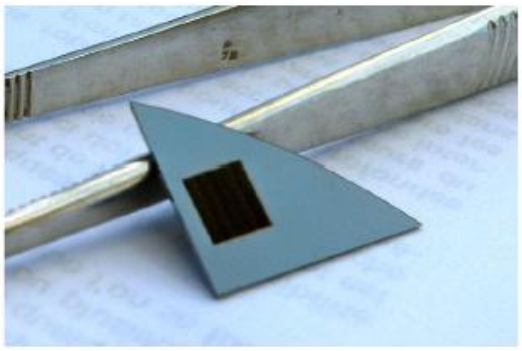

Figure 2.8 : A femtosecond laser stuructured silicon [53].

Except silicon, micro/nano structuring is performed in diverse materials [41,54-57]. Titanium is one of them, due to the variety of its applications [36-40,40,54,57,58]. The surface texturing of titanium is carried out by few groups.

Nayak et.al [37] performed experiments in order to produce microcolumns on titanium surface. A regeneratively amplified Spectra Physics Ti:Sapphire femtosecond laser is used which produces laser pulses at 800 *nm* wavelength, 130 *fs* pulse durations. The experiments are performed at 1 kHz repetition rate and 500 *mm* lens is used. They carry out their experiments in air, vacuum and in diverse gas environments. The most sharp and tall microcolumns are formed in vacuum and He gas environments. In vacuum conditions, sharp structures, which have 25 μm heights, are formed in 1.5 J/cm^2 and in He gas environment the sharp structures are formed under 100 mbar to 800 mbar in 2 J/cm^2. It is stated that lower gas pressure favor long structures. In addition, it is indicated that in air conditions the formations are not so sharp as compared to others. Also, they do not observe spikes under SF_6 gas environment. Another study by *Nayak et.al*. [41] is dedicated to observe these microstructures on titanium, aluminium copper, and stainless steel. The experimental setup is same with the previous study [37]. Micro structures are formed on titanium surface between 0.5 J/cm^2 to 1.2 J/cm^2 fluences. The formations of such structures in stainless steel is observed in vacuum, air , He, SF_6 at 100mbar pressure in 1.2 J/cm^2. The spikes are not formed as titanium and also stainless steel in aluminium and copper.

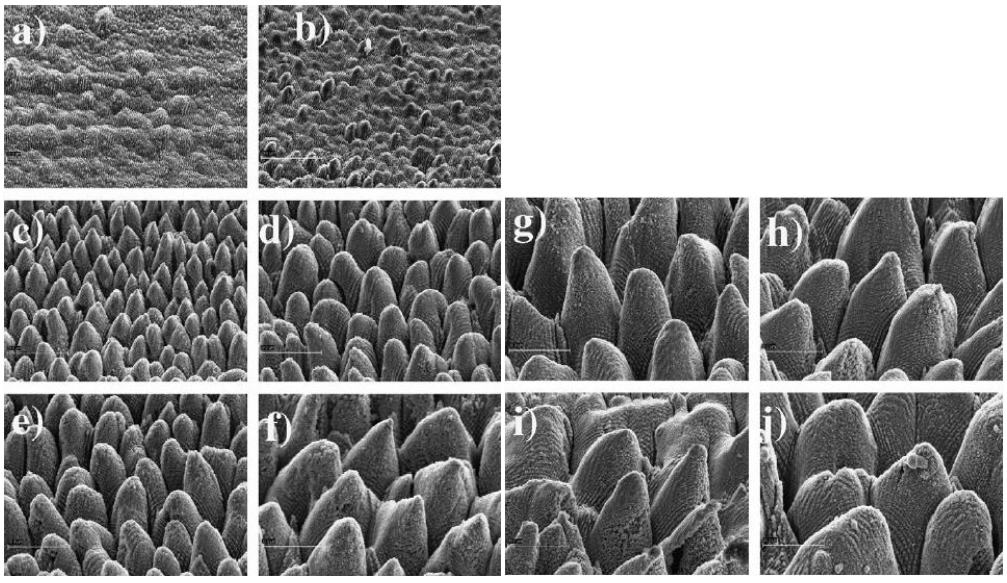

Figure 2.9 : Formations of spikes for (a)0,3 (b) 0,4 (c) 0,5 (d)0,6 (e) 0,7 (f) 0,8 (g) 0,9 (h) 1 (i) 1,1 (j) 1,2 (J/cm^2).The number of laser pulse is 450 [41].

Oliveira et.al. investigated the structuring of titanium under stationary and non-stationary conditions. A commercial Yb:KYW chirped-pulse-regenerative amplification laser system is used which produces pulses at 1030 nm wavelength, 500 fs pulse durations. The non stationary experiments are carried out with 50 Hz repetition rate, where as the stationary experiment conditions varied between 1 Hz and 50 Hz. Figure 2.10 illustrates structuring of titanium under stationary conditions. It is obvious that after 150 pulses at 1 J/cm^2 the structures begin to form, though their formations are not sharp.

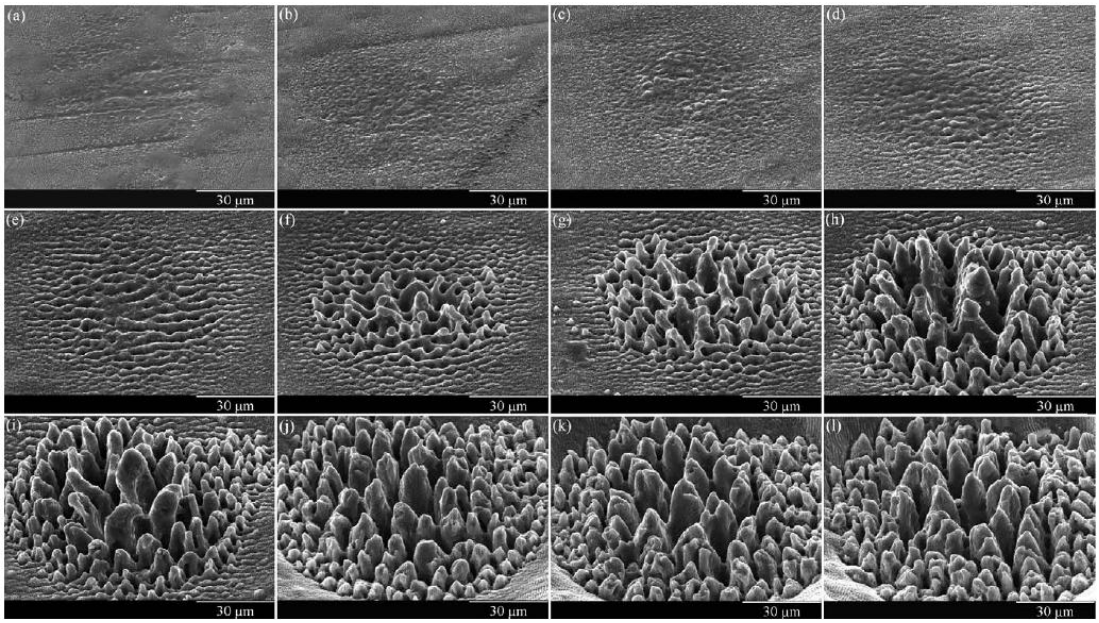

Figure 2.10 : Micro columns on titanium surface under stationary conditions. Fluence is 1 J/cm^2 and number of pulses (a) 1 (b) 5 (c) 10 (d) 20 (e) 50 (f)75 (g) 100 (h) 150 (i) 200 (j) 500 (k) 750 (l)1000 [35].

Figure 2.11 indicates the non-stationary experiments SEM photographs. As seen from the figure that there is formation of micro columns but they are oriented irregular and their formations are not so sharp as compared to other studies. Finally it is stated that the micro columns formation is observed both in stationary and non-stationary conditions [35].

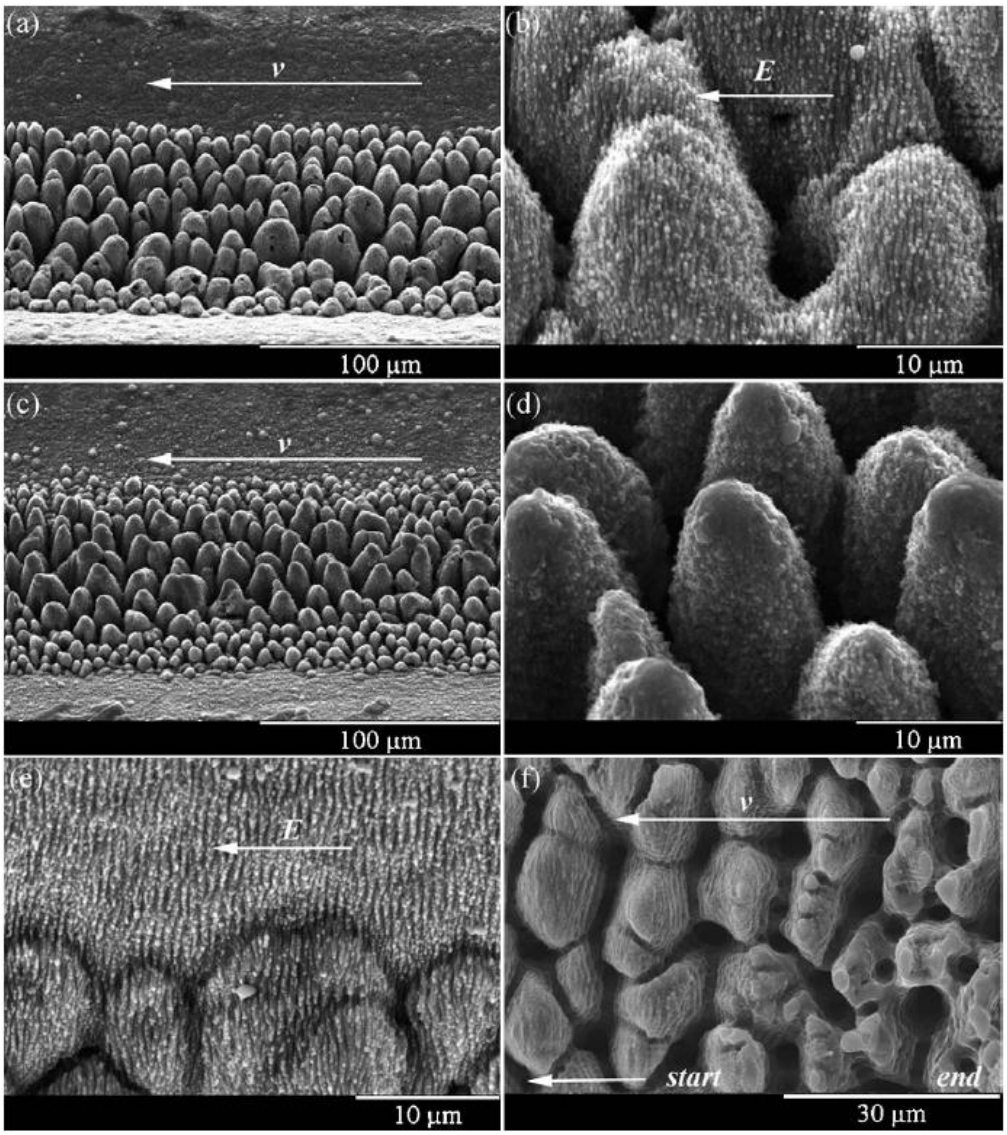

Figure 2.11 : The response of titanium surface under non-stationary conditions. Fluence is 1 J/cm^2 and (a), (b), (e), and(f) 10 µm/s; (c), and (d) 50 µm/s [35].

There are also different applications of surface structuring, for example, cylinder walls in combustion engines. The cavities between the structures serve as a reservoir for the oil and they prevent the breakdown of the oil-film. And finally it results the reduction of particle emission [43].

2.2.1.3 Microfluidic applications

There is a fast growing market for microfluidic technologies and therefore the fabrication process of these devices is getting important [59]. In recent years, femtosecond lasers have significant applications in fabrication of microfluidic devices [22,60-65]. Microfluidic devices increase enhanced signal in single molecule fluorescence detection, which improves sensitivity for biosensor applications [61]. Lab on a chip devices demand three dimensional microchannels which have potential applications in chemical and biological analyses. Femtosecond lasers provide unique advantage of the fabrication of hollow micrometer-diameter three dimensional microfluidic channels in the bulk of transparent materials [60,63]. *Li et.al.* fabricated spiral shaped microchannels in glass in order to connect two microcomponents. In the first step, they investigated the optimum parameters for the fabrication. Then, the microchannels are cut by moving the sample along spiral trace. In the second step, the laser modified area is etched with 5 % HF acid in an ultrasonic bath so as to form hollow structure. Finally, baking is applied to obtain smooth surfaces.

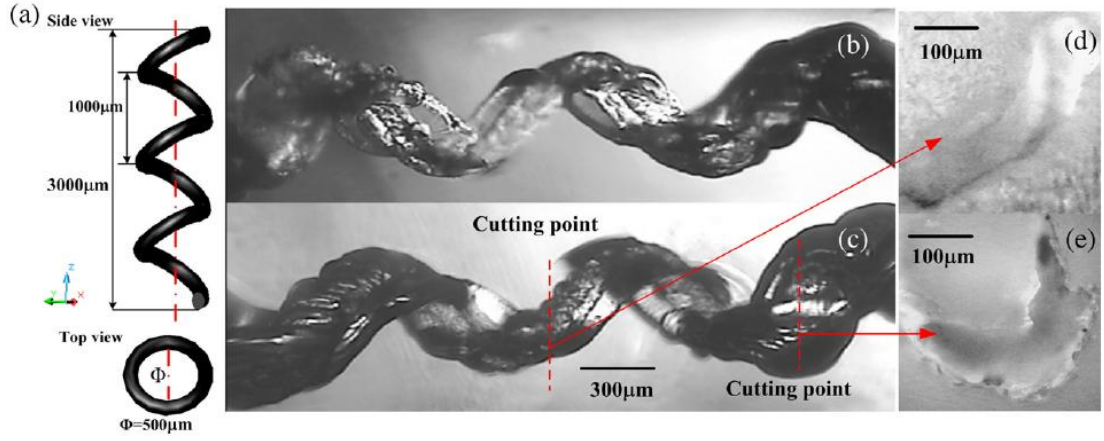

Figure 2.12 : (a)Schematic view of the spiral channel. (b)The microchannel after the etching process. (c) after baking process at 600ºC for 4h. (d) The cross section of the post baked microchannel. (e) The cross section of the channel at the opening area [63].

Figure 2.12 shows the experiment results. It is stated by *Li et.al*. that the etching time, the diameter of the laser modified region and the incidence laser power have influence on the diameter of the channel. They performed liquidity test and produce smooth channel [63].

2.2.2 Biomedical applications

In recent years femtosecond lasers play a significant role in the biomedical applications. The complexity and small feature sizes enhance the necessity of the laser micromachining [66-68]. The biomedical stents are a good application of the femtosecond laser micromachining. These stents are fabricated by a hollow cylindrical tube with a designed pattern. Femtosecond lasers provide unique advantage that various materials can be used to fabricate stents such as stainless steel, nitinol platinium, titanium, tantalum, and gold [47,69,70]. A case study is given in Figure 2.13. This stent is used for cardiovascular surgery and it is produced by tantalum. Laser fabrication process of this stent advantage is that it does not require additional finishing procedures [47].

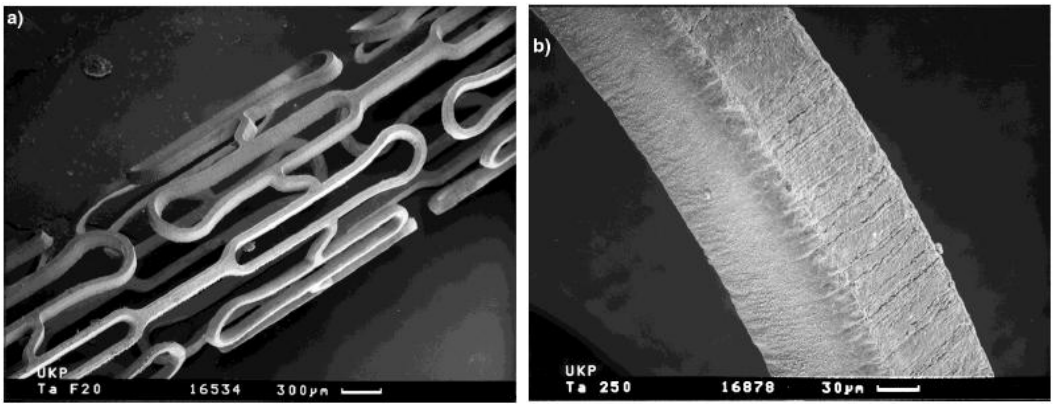

Figure 2.13 : (a) A case study of tantalum stent. (b) Detail of (a) [47].

As discussed in the previous section, texturing the biomedical implant surfaces enhance the cell adhesion and the stability. Further studies are performed on titanium since it has good biocompatibility, durability and frequently used material for the fabrication of biomedical implants [40,68]. *Wang et.al.* used femtosecond laser in order to create micro-patterns on titanium surface. The experiments are performed in simulated body fluid (SBF). After the ablation of the surfaces, an *in vitro* osteoblast culture experiment is performed in order to observe the cell interaction between the patterned surfaces. Figure 2.14 shows the experiment result. In Figure 2.14a the surface is ablated by sand blasting followed by acid etching and the others are ablated by femtosecond laser. The author observe the advantageous of the femtosecond laser ablated (FLA) surface and Figure 2.14d MTT assay results, shows the cell propagation rates on femtosecond laser ablated surfaces are faster than sand blasting followed by acid etching (SLA) surfaces [71].

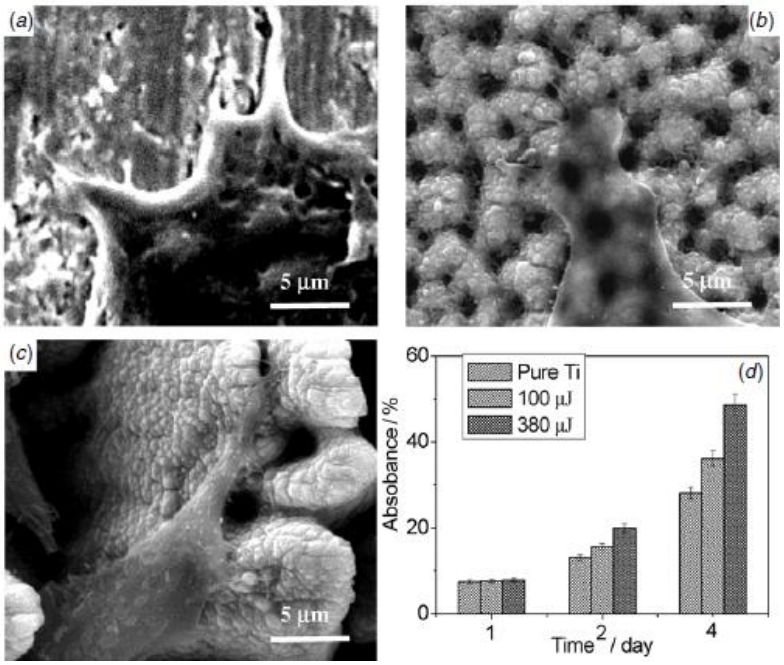

Figure 2.14 : (a) SLA surface (b) FLA surface, fluence 3.3 J/cm^2 (c) FLA surface 12.5 J/cm^2 (d) MTT assay [71].

2.2.3 New applications areas

There are new material trends in the application of femtosecond lasers. In recent years, poly(methyl methacrylate) (PMMA), which is a hard plastic material, exhibits more durability and cheaper as compared to glass have potential applications in the field of microfluidics. Also polymer materials have advantage over glass since they have flexible processing [43]. *Yamasaki et.al.* used PMMA material in order to fabricate microchannels without post-fabrication treatment. Figure 2.15 shows the experiment result. Form Figure 2.15a and 2.15b it is indicated that water solution can penetrate into channels without leakage to the host PMMA. The channels are somewhat elliptical due to the aberrations. The SEM images of the PMMA (Figure 2.15c, 2.15d and 2.15e) show that the channels diameters are about 0.4 and 0.5 μm.

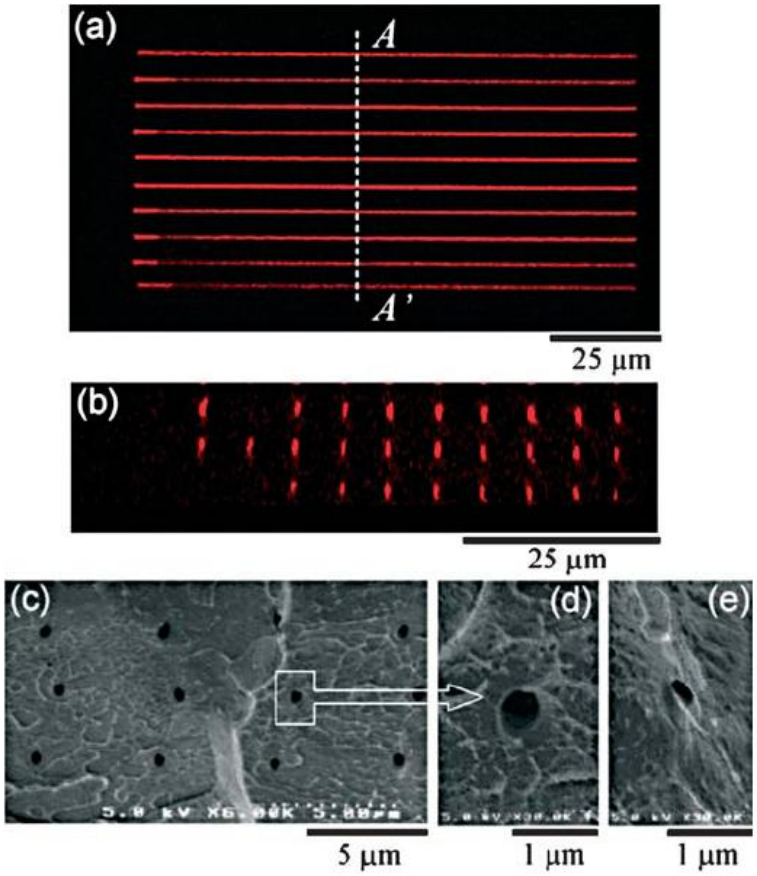

Figure 2.15 : (a) view of channels. (b) views of photoluminescence of rhodamine (c,d) SEM images of the cross section of the channels which were cut 12 nJ (e) 9 nJ [65].

3. EXPERIMENTS AND RESULTS

3.1 Experimental Setup

In our experiments a diode pumped solid state Yb:YAG femtosecond laser (s-Pulse Amplitude Systemes) is used. It is a three level system and produces pulses at 1030 *nm* wavelength, with 500 *fs* pulse width. The experiments are performed at 1 kHz in atmospheric conditions. Since the laser system emits pulses at maximum power, a half wave plate and a polarizer is used in order to change the pulse energy, thus to control the fluence. Figure 3.1 shows the experimental setup.

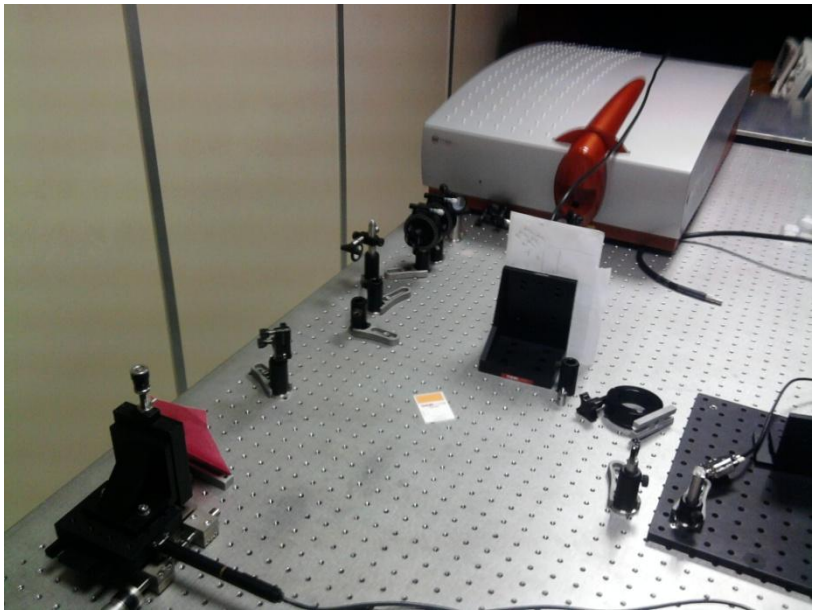

Figure 3.1 : Experimental setup of the femtosecond laser system

3.2 Test Specimen Preparation

High purity (99.9%) titanium materials are diced into small square pieces of $1cm^2$. Before positioning titanium its surface and sides are grinded and then polished with 1 μm alumina liquid. After then the pieces are cleaned with acetone followed by methanol. A computer controlled stage, which has a 100 nm sensitivity, provide precise positioning of titanium plate. The channels are cut from sides so as to view the channel interior view and depth and width. The channels are characterized by SEM (ZEISS EVO|MA10).

3.3 Experimental Studies

The experiments are designed in two categories with sub-sections. Figure 3.2 shows diagram of the experimental design. The experiments are performed by two different focal lengths. In each lens study three different experiments designed and performed.

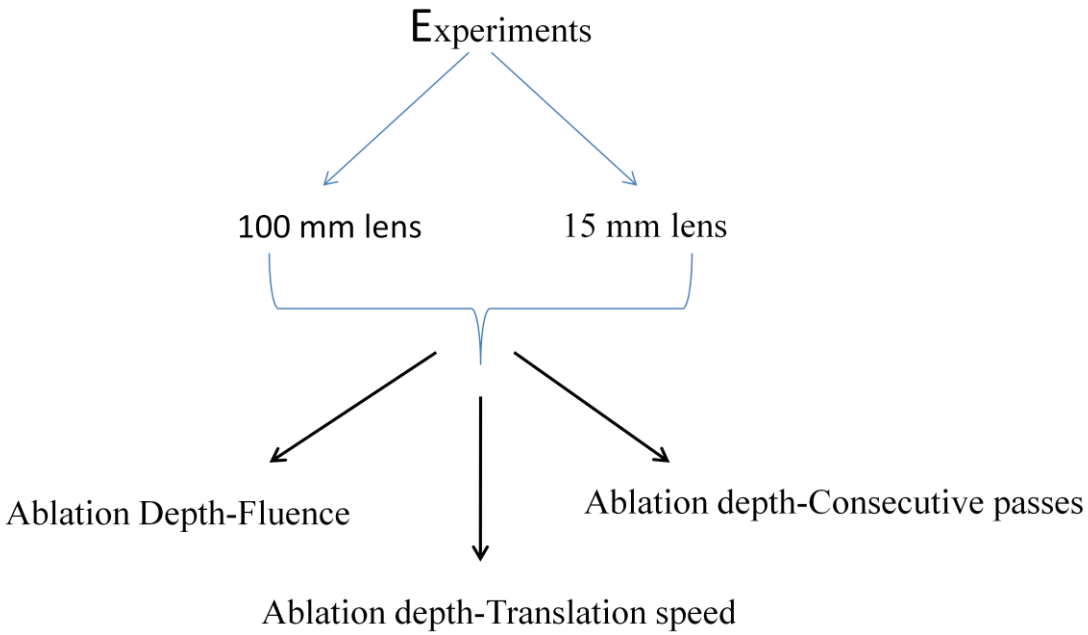

Figure 3.2 : Schematic diagram of the experimental design

3.3.1 Ablation depth-fluence

The main purpose of this step of the experiments is to investigate the effect of the fluence on the ablation depth. Thus, some series of experiments are performed with different fluencies. Firstly, the experiments are performed with 100 *mm* lens (Biconvex-aspherical) and at 1 kHz. The test specimen is located on to the computer controlled stage and moved with constant 10 $\mu m/s$ speed. Table 3.1 indicates the experimental parameters. The power is measured by a thermal power meter and the initial power is 2 *mW* which corresponds to the 2 μJ. The laser beam energy is calculated by the formula;

$$E = \frac{P}{f_{rep}} \qquad \textbf{(3.1)}$$

where E is the laser beam energy, P is the power and f_{rep} is the repetation rate. In order to calculate the fluence, firstly the spot size of the beam is calculated. The spot size relation with the distance from the lens is expressed by equation (**3.2**).

$$w(z) = w_{input}\sqrt{1+\left(\frac{z}{z_R}\right)^2} \tag{3.2}$$

Far away from the waist the relation can be written as;

$$w(z) = w_{input}\sqrt{1+\left(\frac{z}{z_R}\right)^2} \approx w_{input}\sqrt{\left(\frac{z}{z_R}\right)^2} = w_{input}\left(\frac{z}{z_R}\right) \tag{3.3}$$

where w_{input} is the output diameter of the laser beam, z is the distance from the lens and Z_R is the Rayleigh range and can be written as;

$$Z_R = \frac{\pi w_{input}^2}{\lambda} \tag{3.4}$$

where λ is the wavelength of the laser. If we rewrite the equation **(3.3)**

$$w(z) = \frac{\lambda z}{\pi w_{input}} \tag{3.5}$$

The output of the laser beam size at FWHM, is measured by a CCD camera and its spot size, w_{input} is 1 *mm* and the laser beam is nearly Gaussian. A lens will collimate laser beam as illustrated in Figure 3.3 and the new spot size can be calculated by equation **(3.5)**

$$w_f(f) = \frac{\lambda f}{\pi w_{input}} \tag{3.6}$$

where f is the focal length.

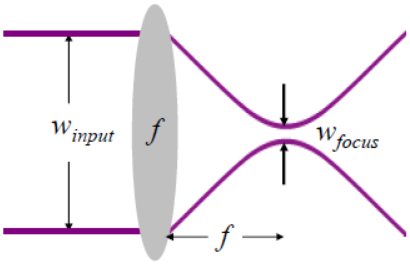

Figure 3.3 : The Gaussian beam is focused to a new spot size [72].

The fluence is calculated using the beam spot size at focal length

$$F = \frac{4E}{\pi w_f^2} \qquad \textbf{(3.7)}$$

The measured power values and the calculated energy and fluence values by equation **(3.1)** and **(3.7)** are given in Table 3.1.

Table 3.1: Experimental parameters for 100 *mm* lens studies

Channel Number	Power [mW]	Energy [μJ]	Fluence [J/cm^2]
1	2	2	0,123
2	3	3	0,185
3	4	4	0,247
4	5	5	0,308
5	6	6	0,370
6	7	7	0,431
7	8	8	0,493
8	9	9	0,555
9	10	10	0,616
10	15	15	0,924
11	20	20	1,233
12	25	25	1,541
13	30	30	1,849
14	35	35	2,157
15	40	40	2,465
16	45	45	2,773
17	50	50	3,081
18	55	55	3,390
19	60	60	3,698
20	65	65	4,006
21	70	70	4,314
22	75	75	4,622
23	80	80	4,930
24	85	85	5,238
25	90	90	5,547
26	95	95	5,855
27	100	100	6,163

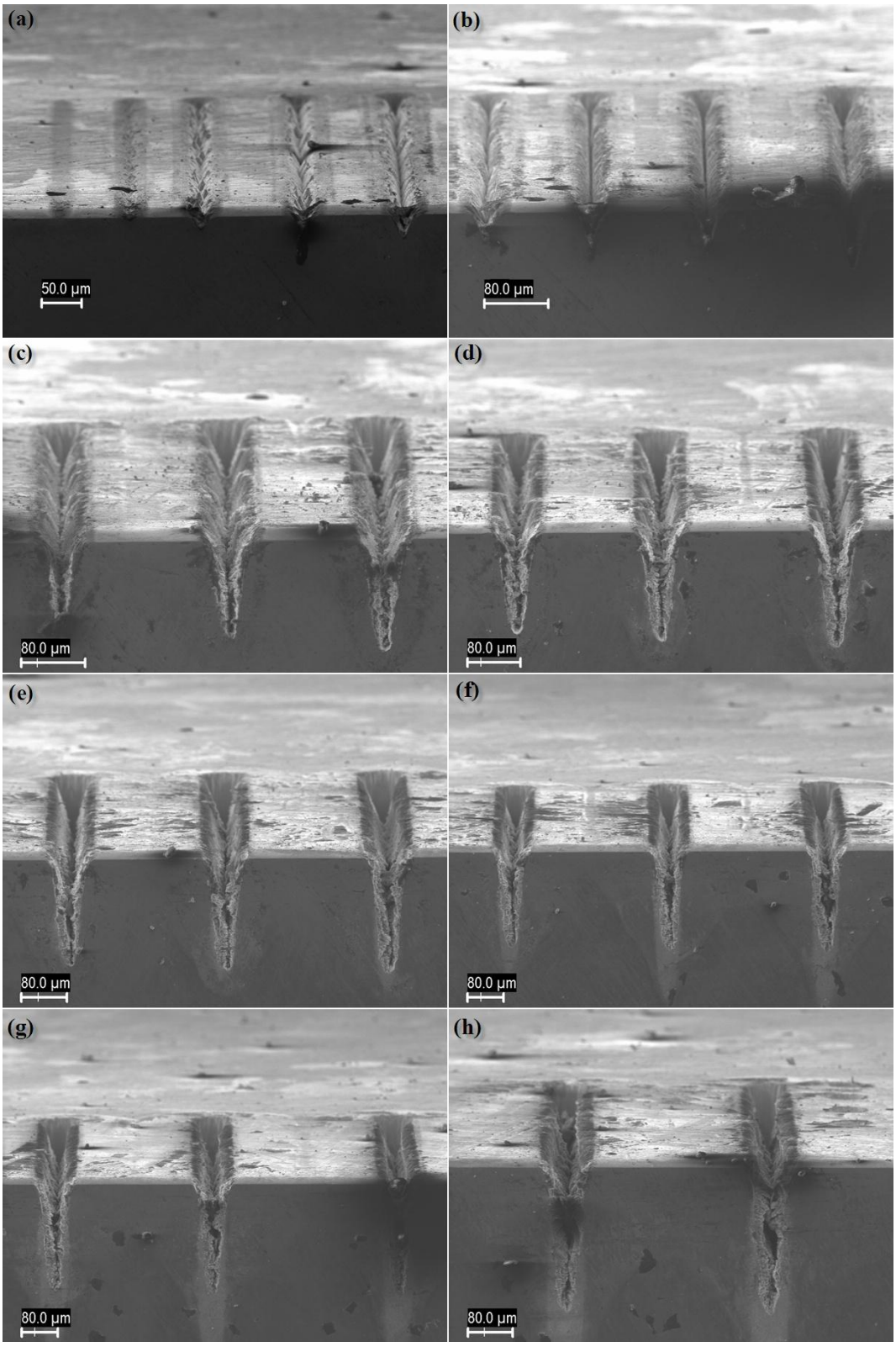

Figure 3.4 : The fluences are in order of (J/cm^2) (a) 0.185-0.431 (b) 0.493-0.92 (c) 1.233-1.849 (d) 2.157-2.773 (e) 3.081-3.698 (f) 4.006- 4.622 (g) 4.930-5.547(h) 5.855, 6.163.

Figure 3.3 illustrates schematic diagram of the focusing collimated Gaussian laser beam to the new spot size. Figure 3.4 shows in order of channels cut at parameters given in Table 3.1. In the lowest fluence 0.123 J/cm^2 titanium was not ablated and the channel was not cut. It is obvious that at lower energies there is no trace of debris around the channels, but at higher energies there are some accumulated debris around the channels and also inside the channels. On the other hand at some small fluencies such as between 0.431-0.616 J/cm^2 the channels walls seem smooth, without any defects on surface. Also, at low fluence values there are some formations of spikes inside the channels. Especially, at 0.308, 0.370, and 0.431 J/cm^2 fluence values the spikes are conspiciously seen. The formations of the spikes are well studied by some research groups in different materials in different gas ambients, such as silicon [48,49,51,52], titanium, aluminum, stainless steel [41]. The fundamental principle behind the formations of these spikes are still unknown. In our case, the experiements are carried out in atmospheric conditions, and the temperature was 25°C.

In the second step, the experiments are performed with a 15 *mm* lens in order to have smaller channels since its spot size is small than 100 *mm* lens' spot size. To compare with previous experiment results, the channels are cut with same fluencies. Since the 15 *mm* lens spot size is smaller than 100 *mm*, this experiment's pulse energy is kept lower than previous study. The 15 *mm* lens study has 6.82 μm spot size, whereas 100 *mm* lens spot size is 45.45 μm which are calculated by equation **(3.6)**. The power and also the energy values are illustrated in Table 3.2 and the power is measured by a Photo diode. In order to measure the power by photo diode, firstly, it is calibrated by thermal power meter in a sufficient high power regime. After then, low power values are measured directly by photo diode. All other experimental conditions are kept same with the 100 *mm* lens study.

Table 3.2: Experimental parameters for 15 *mm* lens studies

Channel Number	Power [mW]	Energy [μJ]	Fluence [J/cm^2]
1	0,046	0,046	0,125
2	0,067	0,067	0,185
3	0,088	0,088	0,242
4	0,111	0,111	0,305
5	0,134	0,134	0,367
6	0,157	0,157	0,430
7	0,182	0,182	0,500
8	0,201	0,201	0,549
9	0,221	0,221	0,606
10	0,337	0,337	0,922
11	0,452	0,452	1,239
12	0,562	0,562	1,539
13	0,675	0,675	1,848
14	0,784	0,784	2,148
15	0,897	0,897	2,458
16	1,014	1,014	2,777
17	1,123	1,123	3,077
18	1,244	1,244	3,407
19	1,353	1,353	3,706
20	1,452	1,452	3,976
21	1,576	1,576	4,316
22	1,685	1,685	4,616
23	1,795	1,795	4,915
24	1,904	1,904	5,215
25	2,017	2,017	5,525
26	2,134	2,134	5,844
27	2,243	2,243	6,144

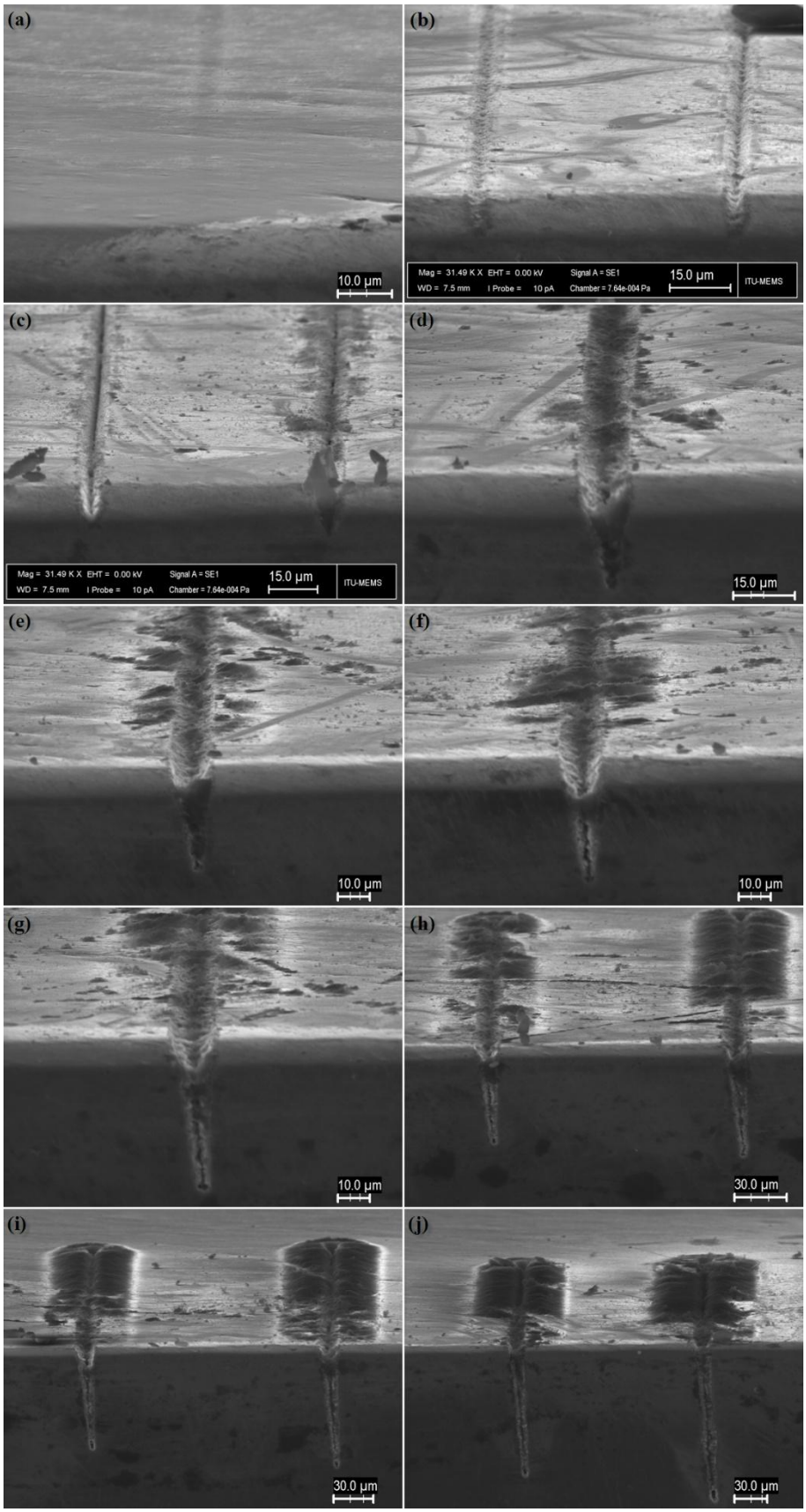

Figure 3.5 : The fluences are in order of (J/cm^2) (a) 0,125 (b) 0,367, 0,430 (c)0,606, 0,921 (d) 2,148 (e) 2,777 (f) 3,407 (g) 3,976 (h) 4,316 (i) 4,915-5,215 and (j) 5,525-5,844.

Figure 3.5 shows SEM photographs of the 15 *mm* lens studies. There are accumulated debris within the channels and also at high fluences debris has accumulated around the top of the channels. Only, the channel, which is cut by 0.606 J/cm^2, can be considered smooth as compared to the other channels in this study, since there is no significant accumulated debris in inside and also outside of the channel. It is important that there are no formations of spikes in channels in this study, though they are cut with same fluences.

The depths are measured under SEM and they are plotted in Figure 3.6. The plot indicates the ablation depth characteristic with different fluence values. Both 15 *mm* and 100 *mm* lens studies' experiment results are given in same plot. The two studies have same characteristics and the data of the two studies were divided into two fluence ranges and a line was fit for each of them. Thus, it can be concluded that there are two different ablation regimes. It is stated by *Nolte et.al.* [1] that optical penetration length is dominant at low fluence regimes, whereas heat diffusion length is active in the high fluence regime. From Figure 3.6 it is obvious that 100 *mm*'s first regime is smaller and also its slope is higher than other regime. As for second regime 15 mm lens slope is bigger than the 100 mm lens study.

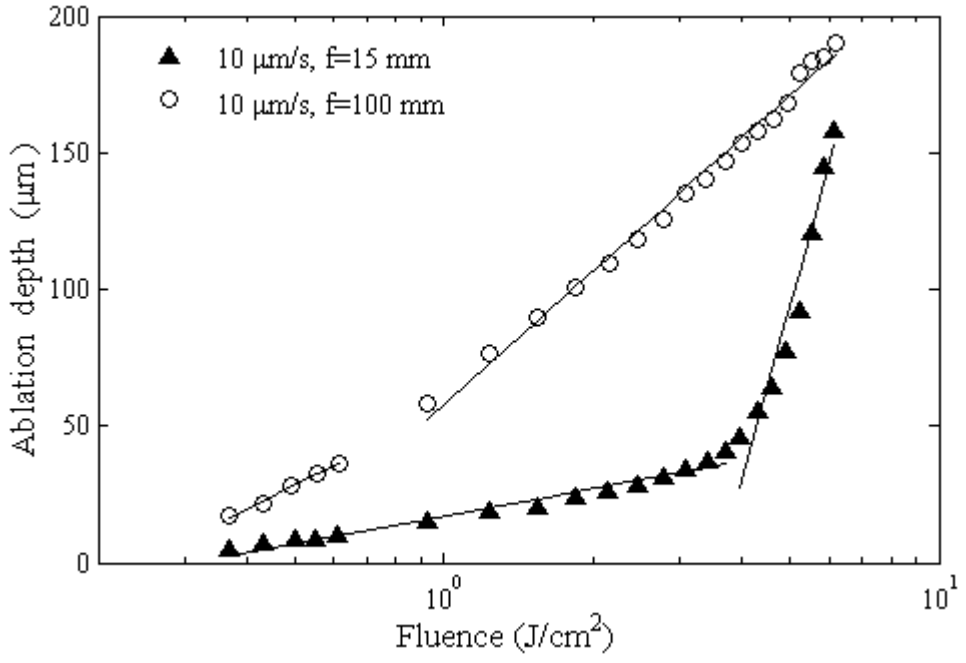

Figure 3.6 : The ablation depth versus fluence

The ablation characteristic is related by the well known expression [1,7,9,10]

$$d = d_o \ln\left(\frac{F}{F_{th}}\right) \quad \textbf{(3.8)}$$

A logarithmic fit to the experimental data gives the d_o and F_{th} values for the two different regimes and Table 3.3 shows the constants. The interesting thing of the graph is that although the channels are cut in same fluencies, the slopes of the ablation regimes are different. One expects to observe same or very few differences of the slopes of two ablation regimes. Therefore, further investigations are need to fully understand the difference between the two different slopes of the studies.

Table 3.3: Fit parameters which are calculated from experiment results

	Low-fluence regime		**High-fluence regime**	
Lens	d_o **[μm]**	F_{th} **[J/cm^2]**	d_o **[μm]**	F_{th} **[J/cm^2]**
15 mm	14,6	0,3123	287,5	3,6104
100 mm	38,7	0,2402	70,3	0,4390

3.3.2 Ablation depth-translational speed

In order to observe the dependence of the channel depth on the translation speed some series of experiments are performed. The pulse energy was held constant at 10 *μJ* in 100 *mm* lens study and 0,224 *μJ* in 15 *mm* lens study, which both of them correspond to 0,616 *J/cm^2*. Translational speeds change from 5 *μm/s* to 200 *μm/s.* Figure 3.7 illustrates the 100 *mm* lens study and Figure 3.8 shows the 15 *mm* lens study.

As seen in Figure 3.7 the channel depth decreases by the increase of translation speed. The smoothest channels are cut at low translation speeds. Especially the channels which are cut 30, 40, 50, 60, 70 *μm/s* translation speeds have a smooth surfaces without accumulated debris. An interior view of channel cut at 50 *μm/s* is given in Figure 3.7(c). The channel walls seem smooth. There are no accumulated debris and also there are no formations of spikes. At high translation speeds the channels are not cut smoothly, only a trace is ablated by Gaussian laser beam.

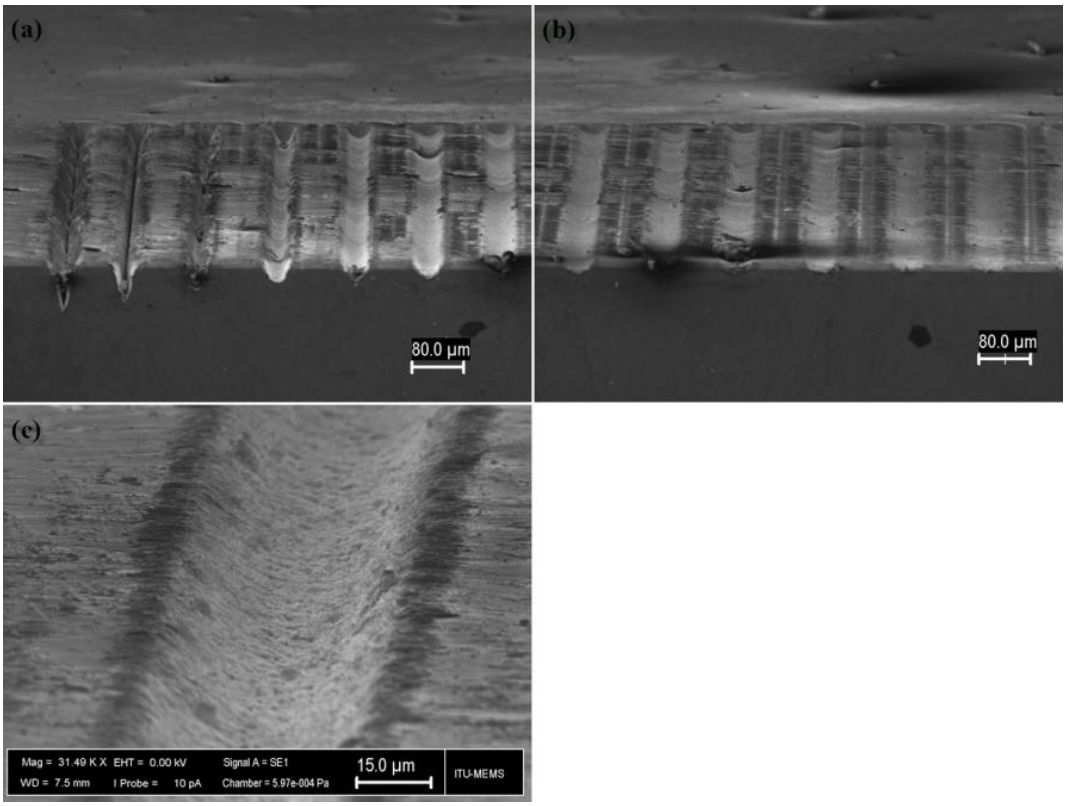

Figure 3.7 : Translation speeds are in order of (*µm/s)* (a) 5, 10, 20, 30, 40, 50, 60 (b)70, 80, 90, 100, 150, 200 (c) interior view of 50 *µm/s* study. Fluence is 0,616 J/cm^2.

Figure 3.8 depicts 15 mm lens SEM photographs. These channels are smaller than 100 mm lens study and there is accumulated debris at low translation speeds. At high translation speeds, with the given fluences, smooth channels cannot be cut. However, at these speeds, it is suitable to microstructure the titanium surface in order to obtain very few sized structures. Figure 3.9 shows an interior view of channel cut at 100 µm/s translation speed. These structures size are about 300 nm and as expressed in section 2.2.2 these small sized structures enhance the stability of bone/implant interface.

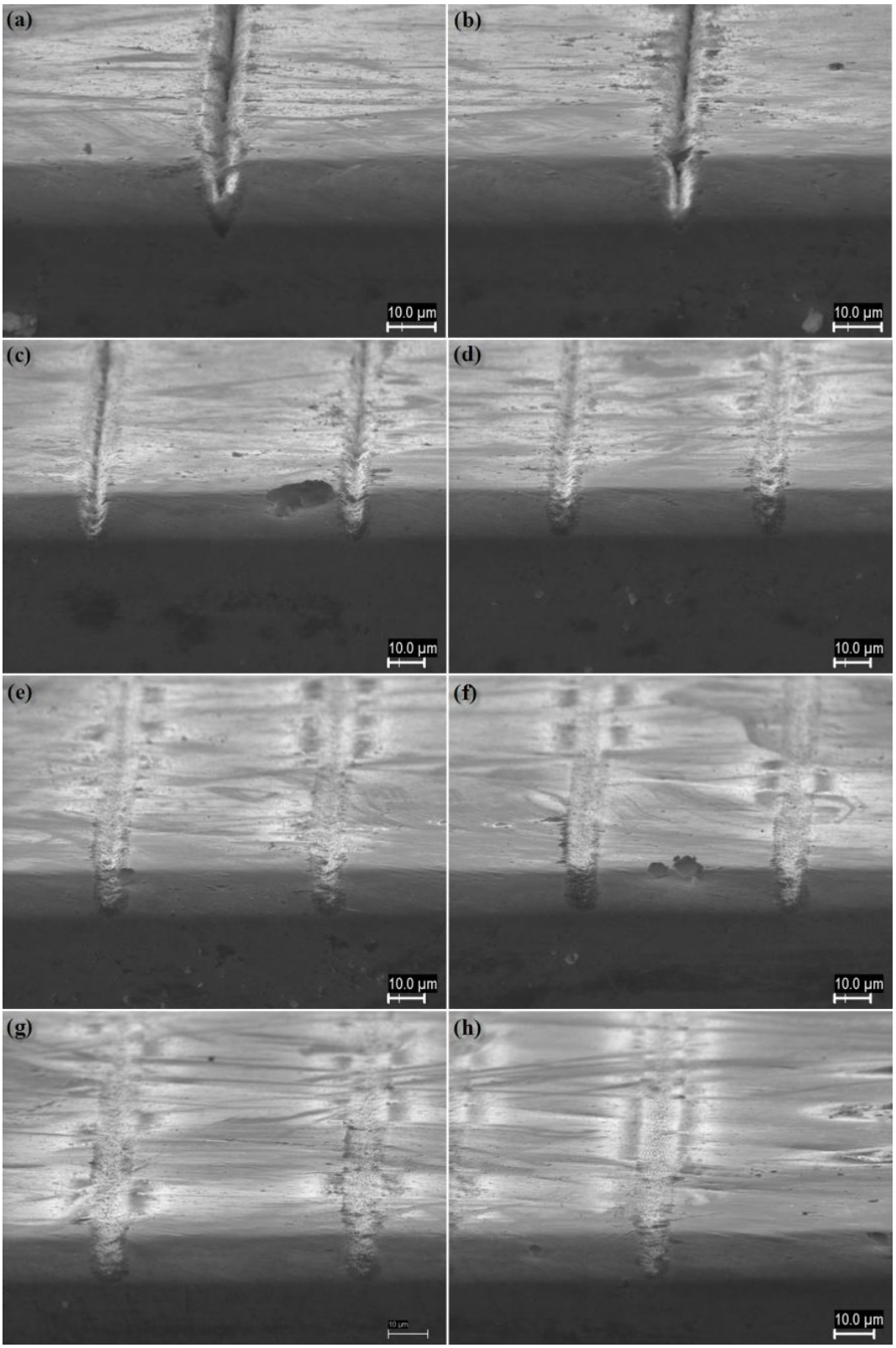

Figure 3.8 : Translation speeds are in order of (*µm/s)* (a) 5 (b)10 (c) 20,30 (d) 40, 50 (e) 60,70 (f)80,90 (g) 100,150 (h)200. Fluence is 0,616 J/cm^2.

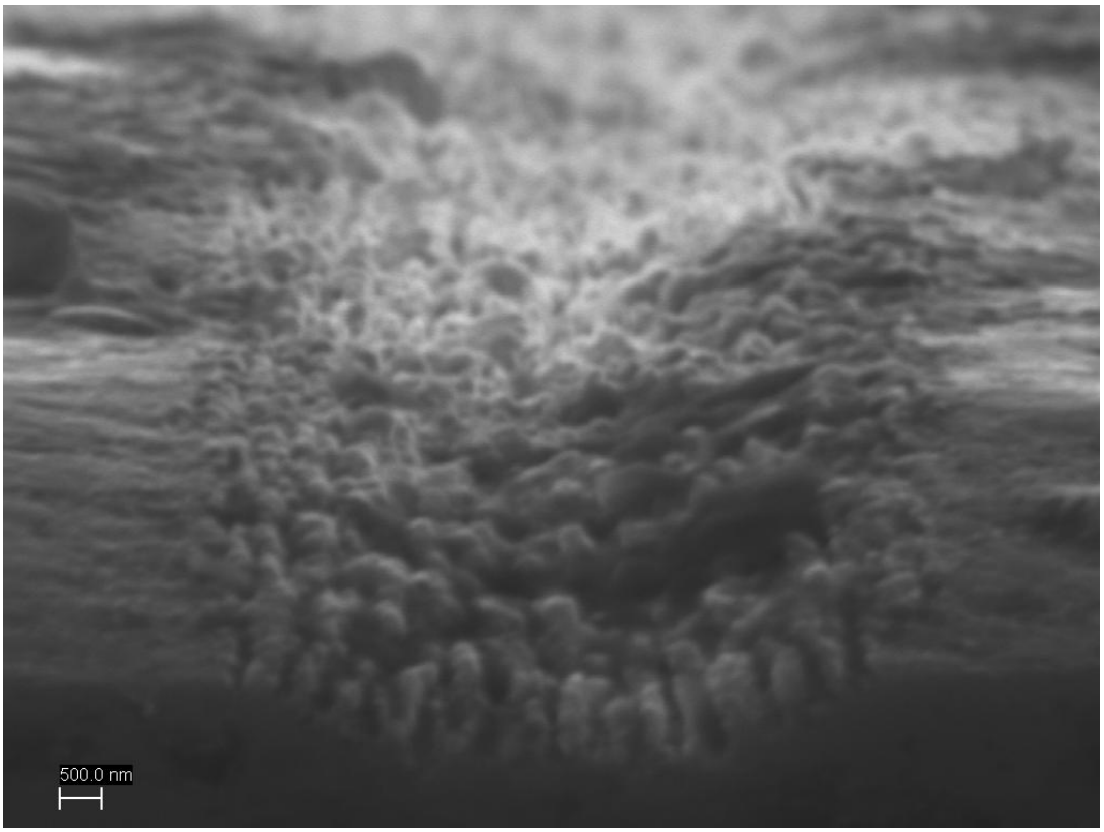

Figure 3.9 : Microstructures on titanium surface. Translation speed is 100 $\mu m/s$.

The ablation depth and translation speed results are plotted and their characteristics are depicted in Figure 3.10. There is an inverse relation between the channel depth and translational speed. This relation can be written by this equation

$$d(v) = \frac{A}{v^k} \tag{3.9}$$

where v is the translation speed, d is the ablation depth and A and k are the fit parameters.

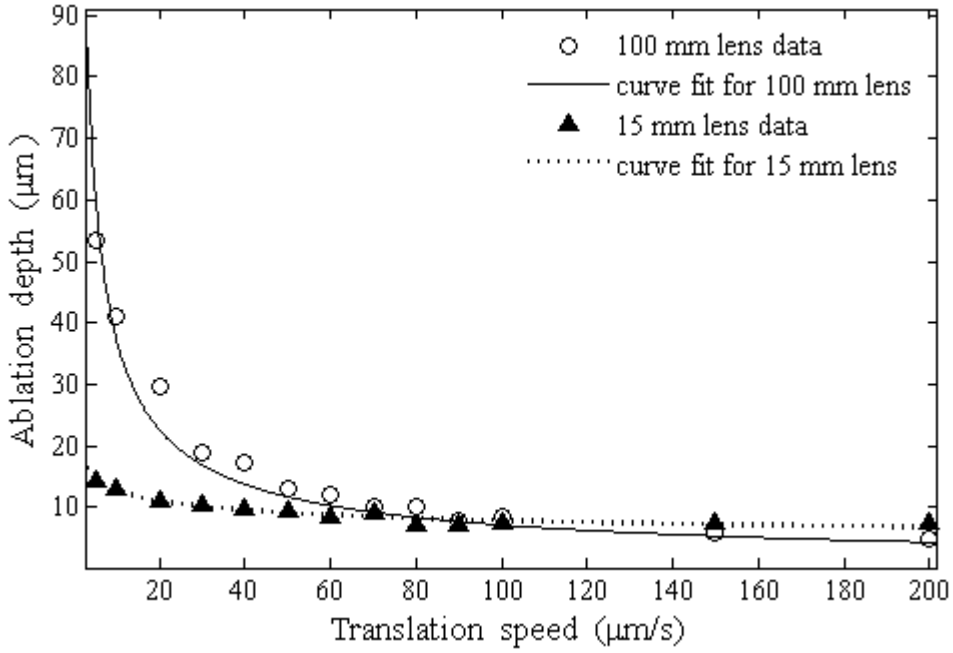

Figure 3.10 : Characteristic of ablation depth with translation speed.

The fit parameters are given in Table 3.4. It is accepted that there are some measurement errors about ± 1μm especially in 15 *mm* lens study at high translation speeds.

Table 3.4: Ablation depth and translation speed fit parameters

Lens	***A* [μm^2/s]**	***k***
15 mm	19,7	0,21
100 mm	214,5	0,72

The test specimen is exposed to multiple pulses while the stage is moving with translation speed *v*. It will be suitable to express a term called "accumulated number of pulses". This term will explain the relation with the multiple pulses with ablation depth. Thus, the ablation depth with translation speed can be expressed in another way. There are different approaches to calculate accumulated number of pulses [8-10], and in this thesis *Ameer-Beg et.al.* approach is used;

$$N_{acc} = \frac{w_f f_{rep}}{v} \qquad \textbf{(3.10)}$$

where w_f is the diameter of the spot size, f_{rep} is the repetition rate, and v is the translation speed. In this approach the number of pulses in a spot size diameter is considered. The results are plotted in Figure 3.11. As expected from Figure 3.10, the ablation depth increases linearly with high accumulated number of pulses, which correspond to low translation speeds. Therefore, the reason for the different slopes can be caused by different accumulated pulses in a spot size. As seen from Figure 3.11, the difference between the maximum and minumum point in 100 *mm* lens is about 8800 pulses, whereas in 15 *mm* lens it is about 1300 pulses.

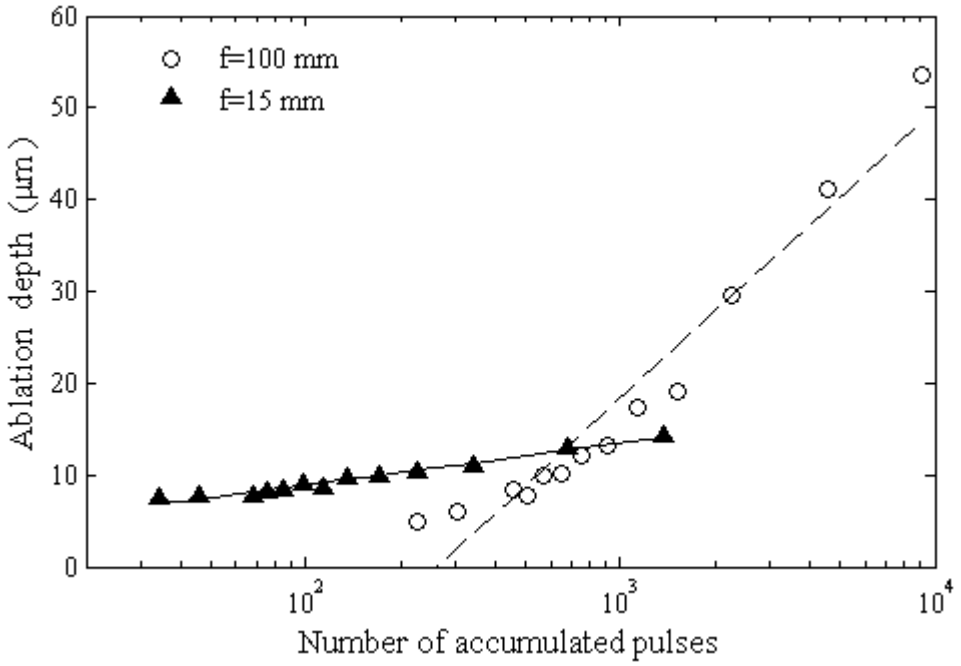

Figure 3.11 : Ablation depth characteristic with accumulated number of pulses.

3.3.3 Ablation depth-number of consecutive passes

It is obvious that consecutive cutting over a material surface will affect the formation of the channel [9,10]. In order to investigate and obtain the parameters effect on the formation of channels some series of experiments are performed. Instead of translating in the same direction, the sample is moved back and forth. The repetition rate was 1 kHz, and the translation speed was 10 *μm/s* in these set of experiments. Firstly, the experiments are performed with 100 *mm* lens. The summary of experimental parameters is given in Table 3.5.

Table 3.5: Experimental parameters for consecutive cutting experiment

Consecutive cutting number	100 mm lens Fluence[J/cm^2]	15 mm lens Fluence [J/cm^2]	
1	0,308	0,308	0,944
5			
10			
15			
20			
25			

As seen from Table 3.5 the 100 *mm* lens study is performed at 0,308 *J/cm^2* fluence which correspond to 5 μJ enerji value and the channels are given in Figure 3.12.

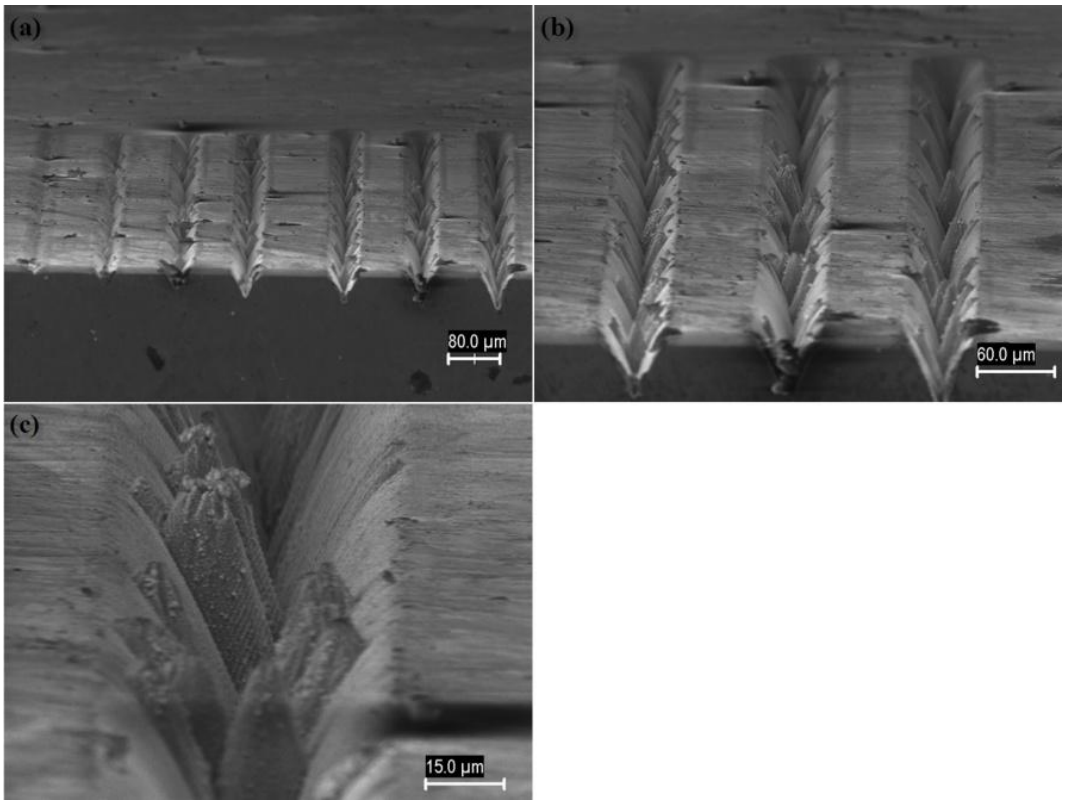

Figure 3.12 : Fluence is 0.308 *J/cm^2* translation speed is 10 $\mu m/s$, consecutive passes are in order of (a)1,1,5,10,15,20,25 (b)magnified view of 15,20,25 cycle (c) interior view of 20 cycle.

It is so evident that there is no accumulated debris both inside and outside of the channels. However, in the same fluence, in ablation depth-fluence study, there was accumulated debris around the channels. Also, there is an important point that the formations of spikes are observed in this study. Especially, in 15, 20, 25 cycle studies the spikes are so clear. Their height is almost same with the channel depth. It is expected that consecutive cutting will melt these microcolumns. However, instead of the eradication of spikes, consecutive passes foster the formations. Also, they oriented irregular inside the channel and some part of them generally base to the channel walls. Their formation mystery is still unclear which are studied by many research groups [48,49,51,52].

Secondly, as indicated in Table 3.5, the 15 *mm* tests are performed in same fluence. The difference from the previous experiments, an additional test is performed in a higher fluence value. Thus, it is anticipated to observe the fluence and the consecutive cutting effect on the formation of spikes. The 0.308 J/cm^2 experiments SEM photographs are shown in Figure 3.13 and 0,944 J/cm^2 fluence experiment results are shown in Figure 3.14.

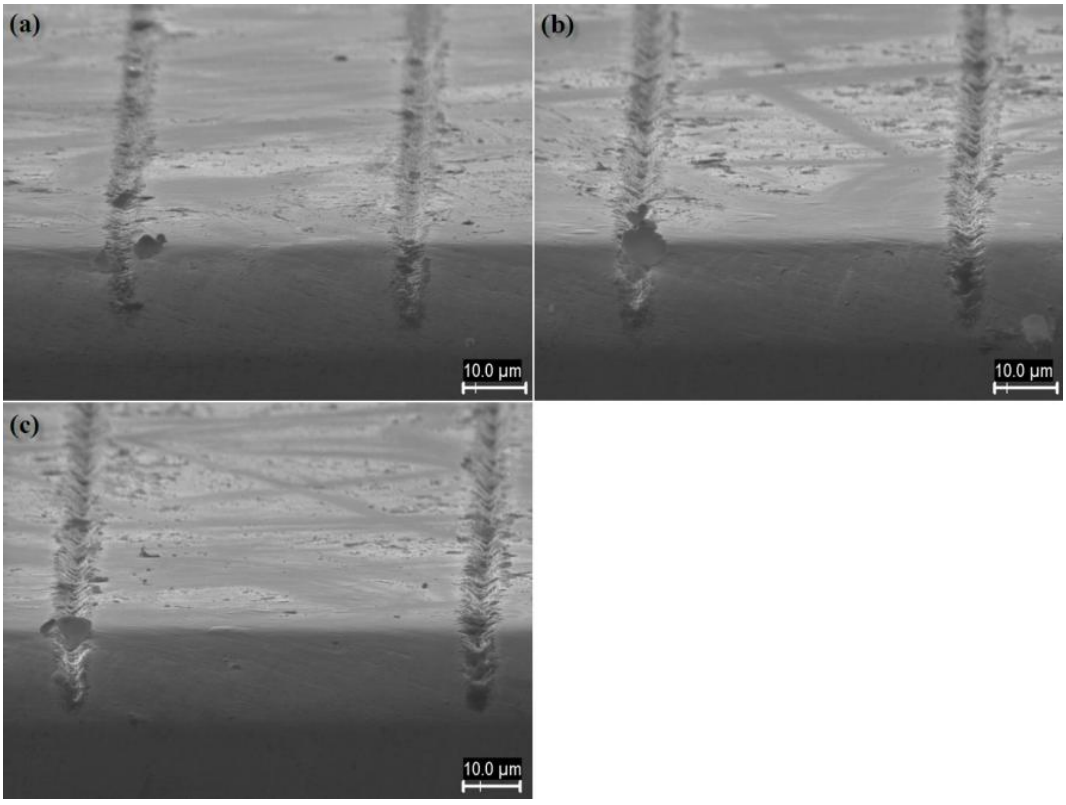

Figure 3.13 : The channels are cut in order of (a)1,5 (b)10,15 (c)20,25 cycles. The fluence is 0.308 J/cm^2.

As seen in Figure 3.13 the channels qualities are not enough smooth. Also there is accumulated debris around the channels and these SEM photographs indicate that at low energies in 15 *mm* lens study the consecutive cutting has no significant effect on the quality of channels. As compared to 100 *mm* lens study the formations of spikes are not observed in this study though all the experimental conditions were same.

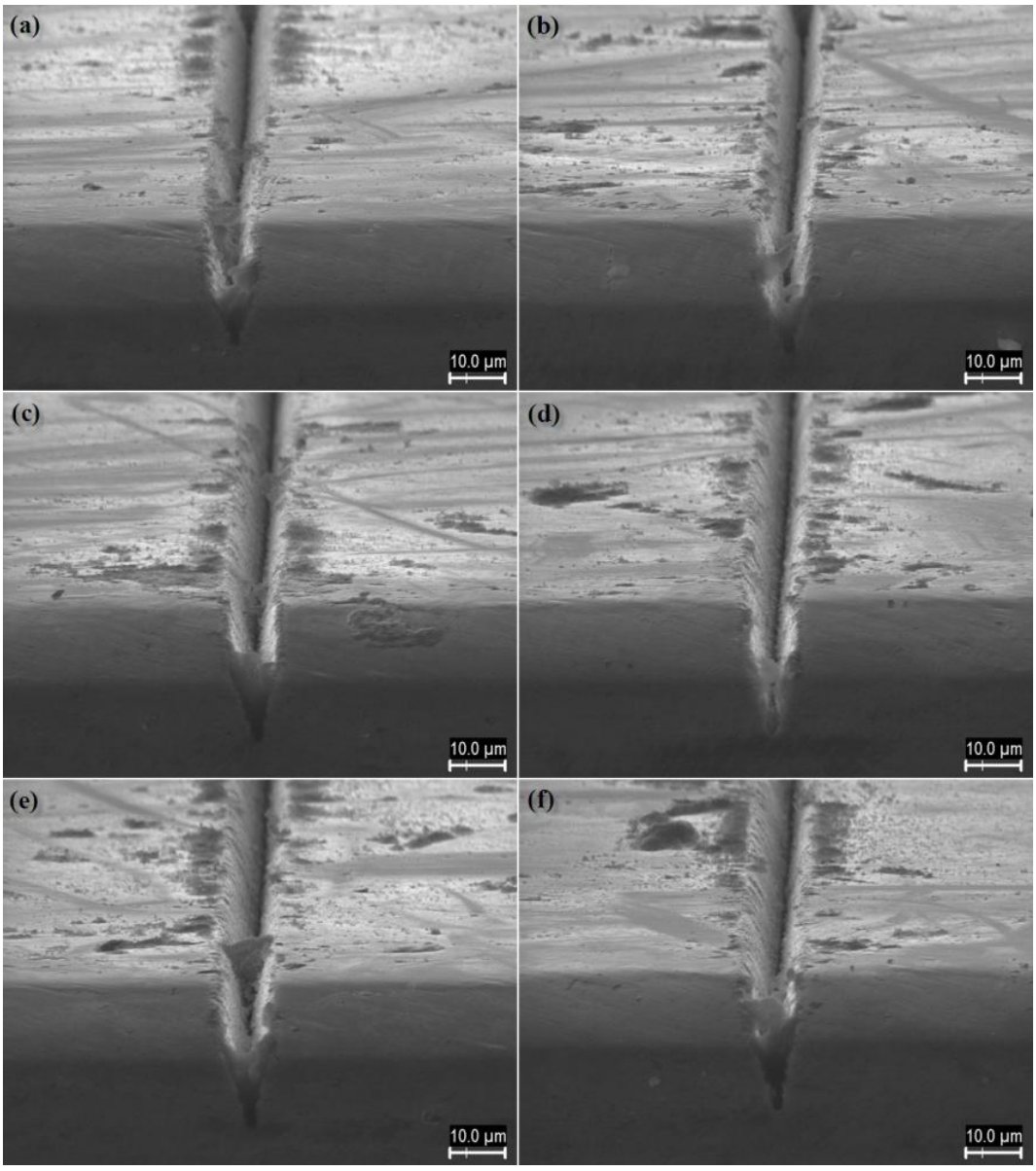

Figure 3.14 : The channels are in order of (a)1 (b)5 (c)10 (d)15 (e)20 (f)25. The fluence is 0.944 J/cm^2.

Figure 3.14 illustrates the consecutive cutting study with 0.944 *J/cm*^{2} fluence. The channels are getting better with the increase of fluence in 15 *mm* lens and in all cases there is a few amount of accumulated debris around the channel. The interesting thing is that the formations of spikes are not observed in these studies.

The experiment results are plotted in Figure 3.15. There is a linear relation in all experiments. The 100 *mm* lens study's slope is higher than the 15 *mm* lens studies in the same fluence values. The reason for the different slopes for the same fluence value and translation speed is due to distinct Rayleigh ranges in addition to the optical penetration depth and the heat diffusion length where the 100 *mm* lens has a smaller optical penetration depth and longer heat diffusion length whereas the 15 *mm* has the opposite as discussed in Figure 3.6. For the 100 *mm* lens Rayleigh range is about 1575 μm, whereas the 15 *mm* lens Rayleigh range is about 35 μm. Therefore, 100 *mm* lens can preserve its spot size, and fluence, longer than 15 *mm* lens.

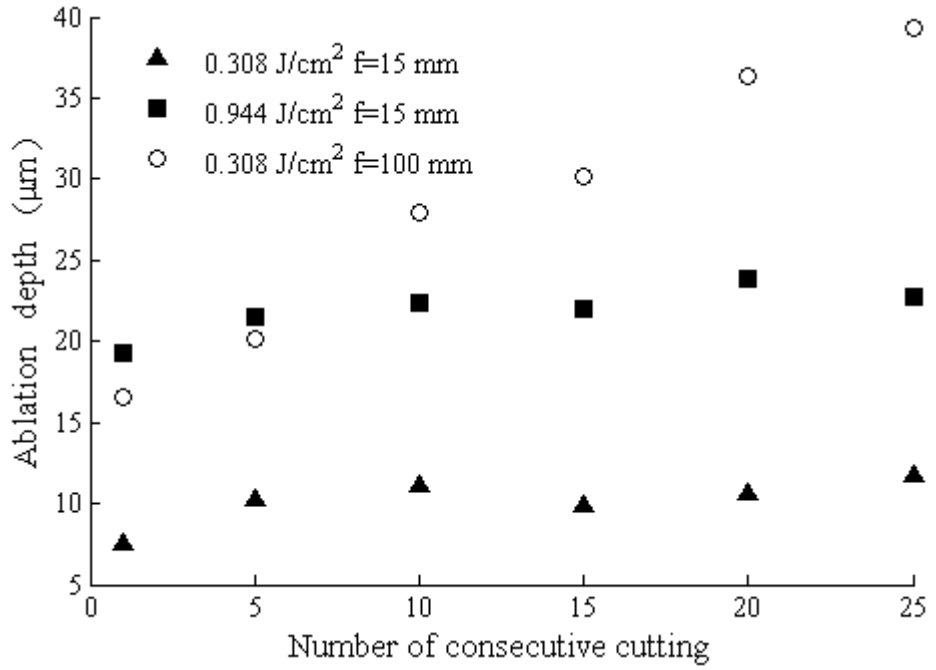

Figure 3.15 : Ablation depth versus consecutive passes over a channel.

The second experiment is designed in order to investigate the reason behind the formation of the spikes. Therefore, some channels are cut in different fluences with 100 *mm* lens and 20 consecutive passes, since the most observable spikes were formed in 20 cycles in our previous experiment. Figure 3.16 shows the result of the experiment. In this step the spike formation is not observed in all different fluencies.

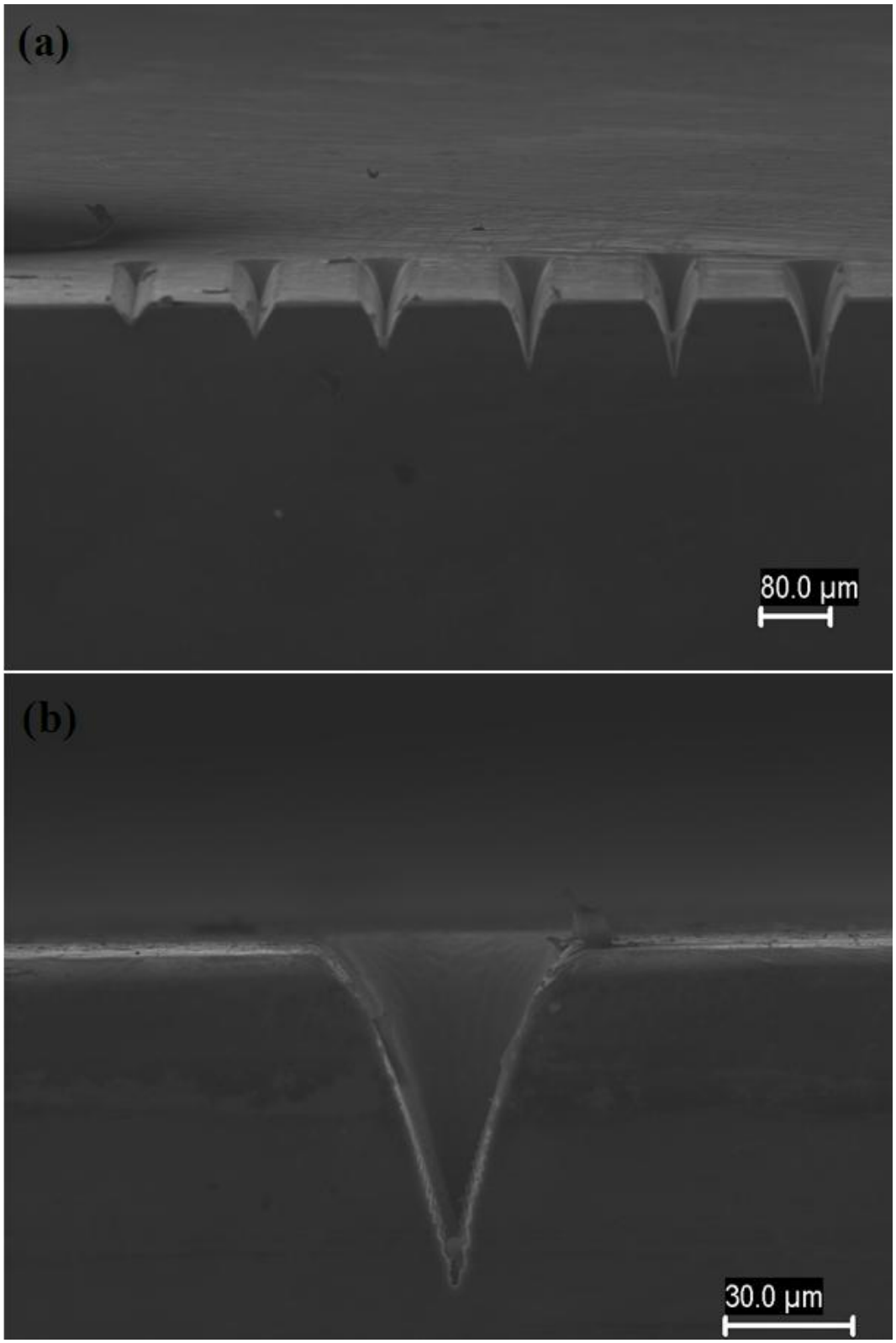

Figure 3.16 : The channels are cut at 20 cycles. (a) The channels are in order of 0.247, 0.308, 0.370, 0.431, 0.493, 0.616 *J/cm*^{2}. (b) An interior view of 0.431 *J*/cm^2.

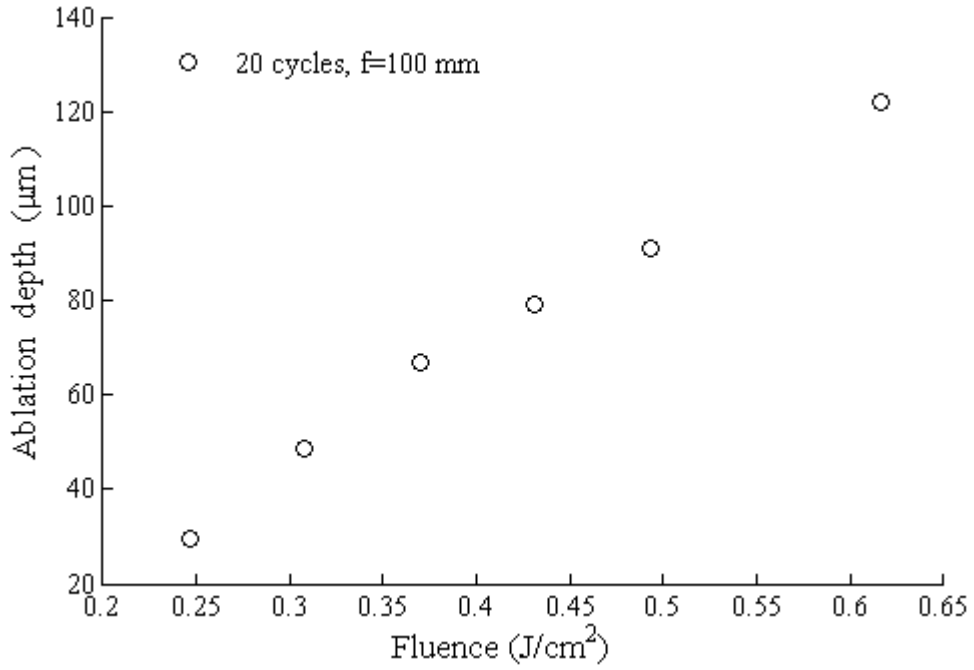

Figure 3.17 : The channels are cut at 20 cycles. (a) The channels are in order of 0.247, 0.308, 0.370, 0.431, 0.493, 0.616 J/cm^2. (b) An interior view of 0.431 J/cm^2.

In contrast, the channels are in high quality with no accumulated debris inside and outside of the channel. The walls seem very smooth and there are no formations of small sized structures. Figure 3.17 shows the change of ablation depth with fluence at 20 consecutive passes. As expected, the depth increases linearly with the fluence. These results indicate that consecutive passes have a significant effect on the channel quality, which supports the smoothest channels.

4. CONCLUSIONS AND FUTURE WORK

The ultimate goal of this research was to characterize the ablation depth with pulse energy, translation speed, and consecutive number of pulses in order to obtain the necessary parameters to cut smooth channels without accumulated debris inside and around the channels. Thus, the ablation depth was characterized with fluence (pulse energy), translation speed and consecutive cutting over a channel.

In ablation depth-fluence study;

- ✓ A logarithmic dependence of the channel depth on the laser pulse energy was observed with two different ablation regimes. Although same fluences were used with two different lenses, the ablation regime's slopes were different.
- ✓ 100 *mm* lens had a small optical penetration length with high slope, whereas the 15 *mm* lens was opposite. In addition, 100 *mm* lens had a long heat diffusion length and low slope as compared to 15 *mm* lens study.
- ✓ On the other hand microcolumns which are called generally spikes, were formed in 100 *mm* lens tests in 0.308, 0.370, 0.431, 0.493 J/cm^2 fluences. In contrast, there were no formations of these spikes in 15 *mm* lens study.
- ✓ It is supposed that these formations might have a relation between the optical penetration depth and heat diffusion length. In addition, there is difference between the characteristics of the two lenses that they have different Rayleigh range, which may foster formations of the spikes. 100 *mm* lens Rayleigh range is about 1575 μm whereas 15 *mm* lens has about 35 μm. Therefore, further investigations have to be performed with different focal lengths in order to realize the relation.
- ✓ Smooth channels were obtained at low fluences in both studies. At high fluences debris was accumulated around and inside the channels.

In ablation depth-translation speed study;

- ✓ It is observed that channel depth was inversely related with translation speed.

- ✓ Some smooth channels were obtained in 100 *mm* lens study when the translation speed was 40, 50, 60, and 70 $\mu m/s$. At 15 *mm* lens study, it was observed that small channels can be cut but their qualities are not good as compared to 100 *mm* lens results.
- ✓ At high translation speeds very few sized micro structures are formed. As indicated in previous section (section 2.2.2) these structures enhance durability and performance of the titanium implants. Some experiments can be performed in order to investigate the most suitable parameters to form the necessary microstructures.

In ablation depth-consecutive cutting study;

- ✓ It is observed that the consecutive number of pulses has a significant effect on the channel formation.
- ✓ The smoothest channels were obtained in consecutive cutting studies while the consecutive passes was 20 and the fluences were 0.247, 0.308, 0.370, 0.431, 0.493, 0.616 J/cm^2 in 100 *mm* lens study.
- ✓ On the other hand, in 15 *mm* lens study at low fluence, 0.308 J/cm^2, smooth channels were not cut. In the second test at high fluence, 0.944 J/cm^2, the channels were smooth as compared to low fluence study, but as not enough as 100 *mm* lens.
- ✓ The spikes were formed in 100 *mm* lens study while the fluence was 0.308 J/cm^2 and they were so clear in 15, 20 and 25 cycles. There were no formations in 15 *mm* lens. As stated previously, they may have a relation with Rayleigh range.

Future Work

- ✓ The formations of microcolums, or spikes, may have a relation with Rayleigh range. Therefore, it will be suitable to perform systematic study with different focal lengths.
- ✓ In this thesis, it is investigated that smooth and small sized micro channels can be cut on titanium materials surface. The smoothest channels are obtained in low fluence, low translation speed, and at high consecutive cutting. For a future work, long, shaped channels can be cut for microfluidic applications.

- ✓ It is discovered that very small sized micro structures can be obtained in ablation depth-translation speed study. This type of textured surfaces can enhance biomedical implants biocompatibility. It will be suitable to pursue a systematic study to discover the optimum parameters for texturing the surface.

REFERENCES

[1] **S. Nolte, C. Momma, H. Jacobs, A. Tünnermann, B. N. Chichkov, B. Wellegehausen, and H. Welling**, 1997: Ablation of metals by ultrashort laser pulses, *J. Opt. Soc. Am. B*, **14**, 2716-2722.

[2] **S. K. Sundaram and E. Mazur**, 2002: Inducing and probing non-thermal transitions in semiconductors using femtosecond laser pulses, *Nat Mater*, **1**, 217-224.

[3] **D. von der Linde, K. Sokolowski-Tinten, and J. Bialkowski**, 1997: Laser-solid interaction in the femtosecond time regime, *Applied Surface Science*, **109-110**, 1-10.

[4] **X. Liu, D. Du, and G. Mourou**, 1997: Laser ablation and micromachining with ultrashort laser pulses, *IEEE Journal of Quantum Electronics*, **33**, 1706-1716.

[5] **R. R. Gattass**, 2006: Femtosecond-laser interactions with transparent materials: applications in micromachining and supercontinuum generation, *PhD Thesis*, Harvard University.

[6] **D. M. Krol**, 2008: Femtosecond laser modification of glass, *Journal of Non-Crystalline Solids*, **354**, 416-424.

[7] **J. Bonse, J. M. Wrobel, J. Krüger, and W. Kautek**, 2001: Ultrashort-pulse laser ablation of indium phosphide in air, *Applied Physics A: Materials Science & Processing*, **72**, 89-94.

[8] **S. Ameer-Beg, W. Perrie, S. Rathbone, J. Wright, W. Weaver, and H. Champoux**, 1998: Femtosecond laser microstructuring of materials, *Applied Surface Science*, **127-129**, 875-880.

[9] **T. H. R. Crawford, A. Borowiec, and H. K. Haugen**, 2005: Femtosecond laser micromachining of grooves in silicon with 800 nm pulses, *Applied Physics A: Materials Science & Processing*, **80**, 1717-1724.

[10] **A. Borowiec and H. K. Haugen**, 2004: Femtosecond laser micromachining of grooves in indium phosphide, *Applied Physics A: Materials Science & Processing*, **79**, 521-529.

[11] **N. Bärsch, K. Körber, A. Ostendorf, and K. H. Tönshoff**, 2003: Ablation and cutting of planar silicon devices using femtosecond laser pulses, *Applied Physics A: Materials Science & Processing*, **77**, 237-242.

[12] **T. Matsumura, T. Nakatani, and T. Yagi**, 2007: Deep drilling on a silicon plate with a femtosecond laser: experiment and model analysis, *Applied Physics A: Materials Science & Processing*, **86**, 107-114.

[13] **G. Kamlage, T. Bauer, A. Ostendorf, and B. N. Chichkov**, 2003: Deep drilling of metals by femtosecond laser pulses, *Applied Physics A: Materials Science & Processing*, **77**, 307-310.

[14] **B. N. Chichkov, C. Momma, S. Nolte, F. von Alvensleben, and A. Tünnermann**, 1996: Femtosecond, picosecond and nanosecond laser ablation of solids, *Applied Physics A: Materials Science & Processing*, **63**, 109-115.

[15] **G. Dumitru, V. Romano, H. P. Weber, M. Sentis, and W. Marine**, 2002: Femtosecond ablation of ultrahard materials, *Applied Physics A: Materials Science & Processing*, **74**, 729-739.

[16] **P. S. Banks, M. D. Feit, A. M. Rubenchik, B. C. Stuart, and M. D. Perry**, 1999: Material effects in ultra-short pulse laser drilling of metals, *Applied Physics A: Materials Science & Processing,* **69**, 377-380.
[17] **S. E. Kirkwood, A. C. van Popta, Y. Y. Tsui, and R. Fedosejevs**, 2005: Single and multiple shot near-infrared femtosecond laser pulse ablation thresholds of copper, *Applied Physics A: Materials Science & Processing,* **81**, 729-735.
[18] **A. Zoubir, L. Shah, K. Richardson, and M. Richardson**, 2003: Practical uses of femtosecond laser micro-materials processing, *Applied Physics A: Materials Science & Processing,* **77**, 311-315.
[19] **C. B. Schaffer, A. Brodeur, J. F. García, and E. Mazur**, 2001: Micromachining bulk glass by use of femtosecond laser pulses with nanojoule energy, *Opt. Lett.,* **26**, 93-95.
[20] **H. Varel, D. Ashkenasi, A. Rosenfeld, M. Wähmer, and E. E. B. Campbell**, 1997: Micromachining of quartz with ultrashort laser pulses, *Applied Physics A: Materials Science & Processing,* **65**, 367-373.
[21] **C. Hnatovsky, R. S. Taylor, E. Simova, P. P. Rajeev, D. M. Rayner, V. R. Bhardwaj, and P. B. Corkum**, 2006: Fabrication of microchannels in glass using focused femtosecond laser radiation and selective chemical etching, *Applied Physics A: Materials Science & Processing*, **84**, 47-61.
[22] **C. Li, X. Shi, J. Si, T. Chen, F. Chen, A. Li, and X. Hou**, 2009: Fabrication of three-dimensional microfluidic channels in glass by femtosecond pulses, *Optics Communications,* **282**, 657-660.
[23] **P. Rudolph, J. Bonse, J. Krüger, and W. Kautek**, 1999: Femtosecond- and nanosecond-pulse laser ablation of bariumalumoborosilicate glass, *Applied Physics A: Materials Science & Processing,* **69**, 763-766.
[24] **R. R. Gattass and E. Mazur**, 2008: Femtosecond laser micromachining in transparent materials, *Nat Photon,* **2**, 219-225.
[25] **J. Bonse, S. Baudach, J. Krüger, W. Kautek, and M. Lenzner**, 2002: Femtosecond laser ablation of silicon–modification thresholds and morphology, *Applied Physics A: Materials Science & Processing*, **74**, 19-25.
[26] **D. Ashkenasi, M. Lorenz, R. Stoian, and A. Rosenfeld**, 1999: Surface damage threshold and structuring of dielectrics using femtosecond laser pulses: the role of incubation, *Applied Surface Science,* **150**, 101-106.
[27] **A. P. Singh, A. Kapoor, K. N. Tripathi, and G. R. Kumar**, 2002: Laser damage studies of silicon surfaces using ultra-short laser pulses, *Optics & Laser Technology,* **34**, 37-43.
[28] **C. Momma, S. Nolte, B. N. Chichkov, F. v. Alvensleben, and A. Tünnermann**, 1997: Precise laser ablation with ultrashort pulses, *Applied Surface Science,* **109-110**, 15-19.
[29] **C. B. Schaffer, J. F. García, and E. Mazur**, 2003: Bulk heating of transparent materials using a high-repetition-rate femtosecond laser, *Applied Physics A: Materials Science & Processing,* **76**, 351-354.
[30] **J. F. Herbstman, A. J. Hunt, and S. M. Yalisove**, 2008: Morphologies and nonlinear scaling of laser damage on glass surfaces by tightly focused femtosecond pulses, *Appl. Phys. Lett.,* **93**, 011112-3.
[31] **C. B. Schaffer, A. O. Jamison, and E. Mazur**, 2004: Morphology of femtosecond laser-induced structural changes in bulk transparent materials, *Appl. Phys. Lett.,* **84**, 1441-1443.

[32] **A. Ben-Yakar, R. L. Byer, A. Harkin, J. Ashmore, H. A. Stone, M. Shen, and E. Mazur**, 2003: Morphology of femtosecond-laser-ablated borosilicate glass surfaces, *Appl. Phys. Lett.*, **83**, 3030-3032.
[33] **A. Rosenfeld, M. Lorenz, R. Stoian, and D. Ashkenasi**, 1999: Ultrashort-laser-pulse damage threshold of transparent materials and the role of incubation, *Applied Physics A: Materials Science & Processing*, **69**, 373-376.
[34] **M. Lenzner, F. Krausz, J. Krüger, and W. Kautek**, 2000: Photoablation with sub-10 fs laser pulses, *Applied Surface Science*, **154-155**, 11-16.
[35] **V. Oliveira, S. Ausset, and R. Vilar**, 2009: Surface micro/nanostructuring of titanium under stationary and non-stationary femtosecond laser irradiation, *Applied Surface Science*, **255**, 7556-7560.
[36] **M. Bereznai, I. Pelsöczi, Z. Toth, K. Turzo, M. Radnai, Z. Bor, and A. Fazekas**, 2003: Surface modifications induced by ns and sub-ps excimer laser pulses on titanium implant material, *Biomaterials*, **24**, 4197-4203.
[37] **B. K. Nayak, M. C. Gupta, and K. W. Kolasinski**, 2008: Formation of nano-textured conical microstructures in titanium metal surface by femtosecond laser irradiation, *Applied Physics A: Materials Science & Processing*, **90**, 399-402.
[38] **Y. Yang, J. Yang, C. Liang, H. Wang, X. Zhu, and N. Zhang**, 2009: Surface microstructuring of Ti plates by femtosecond lasers in liquid ambiences: a new approach to improving biocompatibility, *Opt. Express*, **17**, 21124-21133.
[39] **J. Ilgner, S. Biedron, D. Klee, E. Fadeeva, B. Chichkov, and M. Westhofen**, 2009: Femtosecond Laser Microstructuring and Bioactivation of Titanium Surfaces for Middle Ear Ossicular Replacement Prosthesis, in *World Congress on Medical Physics and Biomedical Engineering, September 7 - 12, 2009, Munich, Germany*, **25/8**, 132-135, Springer Berlin Heidelberg.
[40] **J. R. Bush, B. K. Nayak, L. S. Nair, M. C. Gupta, and C. T. Laurencin**, 2011: Improved bio-implant using ultrafast laser induced self-assembled nanotexture in titanium, *J. Biomed. Mater. Res.*, **97B**, 299-305.
[41] **B. K. Nayak and M. C. Gupta**, 2010: Self-organized micro/nano structures in metal surfaces by ultrafast laser irradiation, *Optics and Lasers in Engineering*, **48**, 940-949.
[42] **C. B. Schaffer**, 2001: Interaction of Femtosecond Laser Pulses with Transparent Materials, *PhD Thesis*, Harvard University.
[43] **L. R. Cerami, E. Mazur, S. Nolte, and C. B. Schaffer**, 2007: Femtosecond laser micromachining, in *Ultrafast Optics*, Rick Trebino and Jeff Squier, Trafford Publishing, Victoria, Canada.
[44] **N. B. Dahotre and S. P. Harimkar**, 2008: Laser Micromachining, in *Laser Fabrication and Machining of Materials*, 247-288, Springer, US.
[45] **E. Kannatey-Asibu**, 2008: Laser Cutting and Drilling, in *Principles of Laser Materials Processing*, John Wiley & Sons, Inc.
[46] **A. Prokhorov, V. Konov, I. Ursu, and I. Mihailescu**, 1990: *Laser Heating of Metals*, Adam Hilger, Bristol.
[47] **S. Nolte, G. Kamlage, F. Korte, T. Bauer, T. Wagner, A. Ostendorf, C. Fallnich, and H. Welling**, 2000: Microstructuring with Femtosecond Lasers, *Adv. Eng. Mater.*, **2**, 23-27.
[48] **T.-H. Her, R. J. Finlay, C. Wu, and E. Mazur**, 2000: Femtosecond laser-induced formation of spikes on silicon, *Applied Physics A: Materials Science & Processing*, **70**, 383-385.

[49] **M. Y. Shen, C. H. Crouch, J. E. Carey, and E. Mazur**, 2004: Femtosecond laser-induced formation of submicrometer spikes on silicon in water, *Appl. Phys. Lett.,* **85**, 5694-5696.
[50] **T. Baldacchini, J. E. Carey, M. Zhou, and E. Mazur**, 2006: Superhydrophobic Surfaces Prepared by Microstructuring of Silicon Using a Femtosecond Laser, *Langmuir*, **22**, 4917-4919.
[51] **J. Zhu, G. Yin, M. Zhao, D. Chen, and L. Zhao**, 2005: Evolution of silicon surface microstructures by picosecond and femtosecond laser irradiations, *Applied Surface Science,* **245**, 102-108.
[52] **T.-H. Her, R. J. Finlay, C. Wu, S. Deliwala, and E. Mazur**, 1998: Microstructuring of silicon with femtosecond laser pulses, *Appl. Phys. Lett.*, **73**, 1673-1675.
[53] **M. Halbwax, T. Sarnet, P. Delaporte, M. Sentis, H. Etienne, F. Torregrosa, V. Vervisch, I. Perichaud, and S. Martinuzzi**, 2008: Micro and nano-structuration of silicon by femtosecond laser: Application to silicon photovoltaic cells fabrication, *Thin Solid Films,* **516**, 6791-6795.
[54] **A. Y. Vorobyev and C. Guo**, 2007: Femtosecond laser structuring of titanium implants, *Applied Surface Science,* **253**, 7272-7280.
[55] **N. G. Semaltianos, W. Perrie, P. French, M. Sharp, G. Dearden, and K. G. Watkins**, 2008: Femtosecond laser surface texturing of a nickel-based superalloy, *Applied Surface Science,* **255**, 2796-2802.
[56] **A. Kuznetsov, J. Koch, and B. Chichkov**, 2009: Nanostructuring of thin gold films by femtosecond lasers, *Applied Physics A: Materials Science & Processing,* **94**, 221-230.
[57] **M. Tsukamoto, K. Asuka, H. Nakano, M. Hashida, M. Katto, N. Abe, and M. Fujita**, 2006: Periodic microstructures produced by femtosecond laser irradiation on titanium plate, *Vacuum,* **80**, 1346-1350.
[58] **D. S. Milovanovic, B. B. Radak, B. M. Gakovic, D. Batani, M. D. Momcilovic, and M. S. Trtica**, 2010: Surface morphology modifications of titanium based implant induced by 40 picosecond laser pulses at 266 nm, *Journal of Alloys and Compounds,* **501**, 89-92.
[59] **S. Lee**, 2008: Femtosecond Laser Nanomachining and Applications to Micro/Nanofluidics for Single Cell Analysis, *PhD Thesis*, University of Michigan, Ann Arbor.
[60] **T. N. Kim, K. Campbell, A. Groisman, D. Kleinfeld, and C. B. Schaffer**, 2005: Femtosecond laser-drilled capillary integrated into a microfluidic device, *Appl. Phys. Lett.,* **86**, 201106-3.
[61] **Y. V. White, M. Parrish, X. Li, L. M. Davis, and W. Hofmeister**, 2008: Femtosecond micro- and nano-machining of materials for microfluidic applications, in *Nanoengineering: Fabrication, Properties, Optics, and Devices V,* **7039**, 70390J-10, SPIE, San Diego, CA, USA.
[62] **J. P. McDonald, V. R. Mistry, K. E. Ray, and S. M. Yalisove**, 2006: Femtosecond pulsed laser direct write production of nano- and microfluidic channels, *Appl. Phys. Lett.,* **88**, 183113-3.
[63] **Y. Li and S.-liang Qu**, 2010: Fabrication of spiral-shaped microfluidic channels in glass by femtosecond laser, *Materials Letters*, **64**, 1427-1429.
[64] **D. B. Wolfe, J. B. Ashcom, J. C. Hwang, C. B. Schaffer, E. Mazur, and G. M. Whitesides**, 2003: Customization of Poly(dimethylsiloxane) Stamps by Micromachining Using a Femtosecond-Pulsed Laser, *Adv. Mater.,* **15**, 62-65.

[65] **K. Yamasaki, S. Juodkazis, S. Matsuo, and H. Misawa**, 2003: Three-dimensional micro-channels in polymers: one-step fabrication, *Applied Physics A: Materials Science & Processing*, **77**, 371-373.
[66] **P. Miller, R. Aggarwal, A. Doraiswamy, Y. Lin, Y.-S. Lee, and R. Narayan**, 2009: Laser micromachining for biomedical applications, *JOM Journal of the Minerals, Metals and Materials Society*, **61**, 35-40.
[67] **S. Schlie, E. Fadeeva, A. Koroleva, A. Ovsianikov, J. Koch, A. Ngezahayo, and B. N. Chichkov**, 2011: Laser-based nanoengineering of surface topographies for biomedical applications, *Photonics and Nanostructures - Fundamentals and Applications*, **9**, 159-162.
[68] **X. Liu, P. K. Chu, and C. Ding**, 2004: Surface modification of titanium, titanium alloys, and related materials for biomedical applications, *Materials Science and Engineering: R: Reports*, **47**, 49-121.
[69] **Y. P. Kathuria**, 2005: Laser microprocessing of metallic stent for medical therapy, *Journal of Materials Processing Technology*, **170**, 545-550.
[70] **N. Grabow, M. Schlun, K. Sternberg, N. Hakansson, S. Kramer, and K.-P. Schmitz**, 2005: Mechanical Properties of Laser Cut Poly(L-Lactide) Micro-Specimens: Implications for Stent Design, Manufacture, and Sterilization, *J. Biomech. Eng.*, **127**, 25-31.
[71] **H. Wang, C. Liang, Y. Yang, and C. Li**, 2010: Bioactivities of a Ti surface ablated with a femtosecond laser through SBF, *Biomedical Materials*, **5**, 1-5.
[72] **S. Aktürk**, 2010: Lasers and Photonics, *Lecture Notes.*

CURRICULUM VITAE

Candidate's full name: Vural Kara

Place and date of birth: Aşkale February 3, 1986

Permanent Address: İTU Mechanical Engineering Faculty, Mechanical Properties of Materials Laboratory, No:240, Gümüşsuyu, İstanbul TURKEY

Universities and Colleges attended: B.Sc., İstanbul Technical University, Mechanical Engineering (2009)

Publications:

- Kara, V., Kizil, H., "Titanium micromachining by femtosecond laser", *Submitted.*